



**HAL**  
open science

## On the combination of the planktonic foraminiferal Mg/Ca, clumped ( $\Delta 47$ ) and conventional ( $\delta 18\text{O}$ ) stable isotope paleothermometers in palaeoceanographic studies

Marion Peral, Franck Bassinot, Mathieu Daëron, Dominique Blamart, Jérôme Bonnin, Frans Jorissen, Catherine Kissel, Elisabeth Michel, Claire Waelbroeck, Helene Rebaubier, et al.

### ► To cite this version:

Marion Peral, Franck Bassinot, Mathieu Daëron, Dominique Blamart, Jérôme Bonnin, et al.. On the combination of the planktonic foraminiferal Mg/Ca, clumped ( $\Delta 47$ ) and conventional ( $\delta 18\text{O}$ ) stable isotope paleothermometers in palaeoceanographic studies. *Geochimica et Cosmochimica Acta*, 2022, 339, pp.22-34. 10.1016/j.gca.2022.10.030 . hal-04291869

**HAL Id: hal-04291869**

**<https://hal.science/hal-04291869>**

Submitted on 17 Nov 2023

**HAL** is a multi-disciplinary open access archive for the deposit and dissemination of scientific research documents, whether they are published or not. The documents may come from teaching and research institutions in France or abroad, or from public or private research centers.

L'archive ouverte pluridisciplinaire **HAL**, est destinée au dépôt et à la diffusion de documents scientifiques de niveau recherche, publiés ou non, émanant des établissements d'enseignement et de recherche français ou étrangers, des laboratoires publics ou privés.

1           **On the combination of the planktonic foraminiferal Mg/Ca, clumped ( $\Delta_{47}$ ) and**  
2           **conventional ( $\delta^{18}\text{O}$ ) stable isotope paleothermometers in palaeoceanographic studies**

3  
4 Marion Peral<sup>1,2</sup>, Franck Bassinot<sup>1</sup>, Mathieu Daëron<sup>1</sup>, Dominique Blamart<sup>1</sup>, Jérôme Bonnin<sup>3</sup>,  
5 Frans Jorissen<sup>4</sup>, Catherine Kissel<sup>1</sup>, Elisabeth Michel<sup>1</sup>, Claire Waelbroeck<sup>5</sup>, Helene  
6 Rebaubier<sup>1</sup> and William R Gray<sup>1</sup>

7  
8 (1) Laboratoire des Sciences du Climat et de l'Environnement, LSCE/IPSL, CEA-CNRS-UVSQ, Université  
9 Paris-Saclay, France

10 (2) Now at Analytical-Environmental and Geo-Chemistry, Vrije Universiteit Brussel, Belgium

11 (3) Université de Bordeaux, CNRS, Environnements et Paléoenvironnements Océaniques et  
12 Continentaux (EPOC), UMR 5805, Allée Geoffroy St Hilaire, 33615 Pessac Cedex, France

13 (4) UMR CNRS 6112 LPG-BIAF Bio-Indicateurs Actuels et Fossiles, Université d'Angers, 2, Boulevard  
14 Lavoisier, 49045 Angers Cedex, Franc

15 (5) LOCEAN/IPSL, Sorbonne Université-CNRS-IRD-MNHN, UMR7159, Paris, France  
16

17 **Abstract**

18  
19 Assuming that foraminiferal clumped isotope ( $\Delta_{47}$ ) values are independent of seawater salinity  
20 and pH, the combination of Mg/Ca,  $\delta^{18}\text{O}$  and  $\Delta_{47}$  values, may in theory allow us to disentangle  
21 the temperature, salinity/ $\delta^{18}\text{O}_{\text{sw}}$  and pH signals. Here, we present a new Mg/Ca- $\Delta_{47}$  dataset  
22 for modern planktonic foraminifera, from various oceanographic basins and covering a large  
23 range of temperatures (from 0.2 to 25.4 °C). These measurements were performed on the  
24 same samples and species as the ones used for the foraminiferal  $\Delta_{47}$  calibration of Peral et al.  
25 (2018), allowing comparison between both Mg/Ca and  $\Delta_{47}$  paleothermometers (excluding the  
26 two benthic foraminiferal data points). There is a good agreement between these two  
27 paleothermometers when the Mg/Ca-temperature is corrected for seawater salinity and pH,  
28 suggesting that foraminiferal  $\Delta_{47}$  may not be influenced by salinity or pH. However, our results  
29 show that  $\Delta_{47}$  temperature uncertainties still limit our ability to reconstruct pH and  $\delta^{18}\text{O}_{\text{sw}}$   
30 from the combination of Mg/Ca,  $\delta^{18}\text{O}$  and  $\Delta_{47}$  in a useful manner. We also find that  
31 disagreements between Mg/Ca and  $\Delta_{47}$  values in *G. bulloides* persist after correction for vital,  
32 salinity and pH effects, suggesting that other process(es) may also influence Mg/Ca in this  
33 species.

34 This study also provides an updated I-CDES version of the previously published planktonic and  
35 benthic foraminiferal  $\Delta_{47}$  calibration of Peral et al. (2018) , covering a range of temperature  
36 from -2 to 25.4 °C.

37

## 38 1. INTRODUCTION

39

40 The reconstruction of key physical and chemical ocean water parameters, like  
41 seawater temperature, salinity and pH, is critical to understand the processes driving past  
42 ocean and climate variations. However, precisely quantifying these parameters remains  
43 extremely challenging. Several proxies have been developed to reconstruct paleo-  
44 temperatures, but they all suffer from various limitations and biases. In his seminal work on  
45 isotopes, Harold Urey suggested that the extent by which  $^{18}\text{O}$  was enriched in marine calcium  
46 carbonates relative to the water from which it is precipitated, could be used as a past ocean  
47 thermometer (Urey, 1947). However, later studies showed that this paleo-thermometer is  
48 biased by the isotopic composition of the global ocean ( $\delta^{18}\text{O}_{\text{sw}}$ ) that does not remain constant  
49 but reflects the waxing and waning of large continental ice sheets over glacial and interglacial  
50 cycles. This signal associated with global changes in continental ice volume strongly imprints  
51 paleo- $\delta^{18}\text{O}$  records obtained from marine carbonates (Shackleton, 1967), with additional  
52 contributions from regional modifications of evaporation/precipitation to a lesser degree.  
53 Thus, it is impossible to accurately reconstruct past ocean temperature using the carbonate  
54  $\delta^{18}\text{O}$ -thermometer without an independent knowledge of seawater  $\delta^{18}\text{O}_{\text{sw}}$ . Furthermore,  
55 interspecies differences in the  $\delta^{18}\text{O}$ -temperature relationship testify to the importance of  
56 physiological processes, also called “vital” effects (e.g. Urey et al., 1951). In order to take into  
57 account these effects, several authors developed species-specific calibrations (e.g., Bemis et  
58 al., 1998; Mulitza et al., 2003).

59 More recently, several studies showed that the Mg/Ca elemental ratio of foraminiferal  
60 calcite can be used to reconstruct paleo-seawater temperatures (Rosenthal et al., 1997; Lea  
61 et al., 1999; Elderfield and Ganseen, 2000). Most foraminiferal species build their shells from  
62 magnesium-poor calcite, in which the minor amount of Mg that can be substituted to Ca is  
63 temperature dependent (Oomori et al., 1987). The paleoclimatology community had great  
64 expectations regarding the combination of foraminiferal  $\delta^{18}\text{O}$  and the Mg/Ca-thermometer,  
65 which could be measured from the same material allowing theoretically to disentangle  
66 temperature and  $\delta^{18}\text{O}_{\text{sw}}$  signals. However, the Mg/Ca-thermometry proved to be more  
67 complex and challenging than originally expected. First, it appeared that the partitioning  
68 coefficient between Mg in seawater and Mg in the crystal matrix is not only

69 thermodynamically controlled by temperature, but also reflects physiological or ecological  
70 processes (Rosenthal et al., 1997; Lea et al., 1999; Elderfield and Ganseen, 2000; Lea, 2014),  
71 prompting several authors to develop species-specific, empirical Mg/Ca-temperature  
72 calibrations (Nürnberg et al., 1996; Rosenthal et al., 1997; Lea et al., 1999; Erez, 2003). From  
73 the first development of the Mg/Ca paleothermometer it was shown that foraminiferal Mg/Ca  
74 is influenced by physico-chemical variables other than temperature such as bottom-water  
75 carbonate ion concentration (Elderfield et al., 2006; Rosenthal et al., 2006), as well as surface  
76 salinity (Nürnberg et al., 1996; Lea et al., 1999; Kisakürek et al., 2008; Mathien-Blard and  
77 Bassinot; 2009, Gray et al., 2018; Gray and Evans, 2019) and pH (Lea et al., 1999; Gray et al.,  
78 2018; Gray and Evans 2019), and - on time-scales longer than  $\sim 1$  Ma - the Mg/Ca ratio of  
79 seawater (Evans et al, 2016). In addition, analytical procedures must be carefully considered  
80 since cleaning protocols have an effect on the measurement of Mg/Ca within foraminiferal  
81 shells (Barker et al 2003; Pang et al., 2020 and references therein). These secondary influences  
82 on foraminiferal Mg/Ca complicate its use as a temperature proxy.

83 The carbonate clumped isotope method (noted  $\Delta_{47}$  hereafter) is one of the most recent  
84 paleothermometers, which has been developed over the last decade (Eiler, 2007, 2011). The  
85  $\Delta_{47}$  approach is based on the quantification of subtle statistical anomalies in the abundance  
86 of doubly substituted carbonate isotopologues ( $^{13}\text{C}^{18}\text{O}^{16}\text{O}^{16}\text{O}^{2-}$ ) relative to the random  
87 distribution of isotopes (Eiler, 2007, 2011). A slightly higher abundance of  $^{13}\text{C}^{18}\text{O}$  bonds is, for  
88 thermodynamical reasons, a function of temperature (Eiler, 2011; Passey and Henkes, 2012;  
89 Stolper and Eiler, 2016) and this relationship is independent of the  $\delta^{18}\text{O}$  of water in which the  
90 calcification occurs (Schauble et al., 2006). Clumped isotope methodological studies have  
91 shown no evidence of vital effects (Tripathi et al., 2010; Grauel et al., 2013; Peral et al., 2018;  
92 Piasecki et al., 2019; Meinicke et al., 2020) nor salinity effects (Grauel et al., 2013; Peral et al.,  
93 2018) on foraminiferal  $\Delta_{47}$ . Moreover, studies dealing with non-foraminiferal carbonates  
94 (Tripathi et al., 2015; Watkins and Hunt, 2015) showed a lack of pH effect (or its negligible  
95 influence) on clumped isotope. The absence of major biases would make  $\Delta_{47}$  one of the most  
96 promising paleo-thermometers. However, its use is still limited because of its low temperature  
97 sensitivity and the large sample size required to significantly reduce the analytical  
98 uncertainties. Obtaining precise and high-resolution  $\Delta_{47}$  records remain a challenge.

99           Because of non-thermal effects on Mg/Ca from foraminifer shells, recent comparisons  
100 revealed discrepancies between Mg/Ca- and  $\Delta_{47}$ -derived temperatures (Peral et al., 2020;  
101 Leutert et al., 2020; Meinecke et al., 2021). These discrepancies are not linked to any specific  
102 foraminifer species (different species were used in the three studies), nor are they associated  
103 to a given oceanic basin (samples from three different regions were studied, the  
104 Mediterranean Sea, the Southern Ocean, and the Indian Ocean) or to a time period (the  
105 studies covered from the late Pleistocene to 5 million years ago). We believe that these  
106 discrepancies can be extremely informative as they may chiefly reflect vital effects and the  
107 impact of salinity and pH on the Mg/Ca-thermometer, offering theoretically the opportunity  
108 to disentangle temperature, salinity, and pH from the combination of  $\delta^{18}\text{O}$ , Mg/Ca and  $\Delta_{47}$  in  
109 planktonic foraminifera. Planktonic foraminiferal  $\delta^{18}\text{O}$  depends on temperature and  $\delta^{18}\text{O}_{\text{sw}}$ ,  
110 the latter being correlated with the salinity. Carbonate  $\delta^{18}\text{O}$  may be combined with  $\Delta_{47}$ -  
111 derived temperature to reconstruct the  $\delta^{18}\text{O}_{\text{sw}}$  (Peral et al., 2020). As Mg/Ca is influenced by  
112 salinity and pH, pH may be obtained by paring the Mg/Ca ratio with the reconstructed  
113 temperature from  $\Delta_{47}$  and salinity estimates from sea-level or from the combination of  $\delta^{18}\text{O}$ -  
114  $\Delta_{47}$ , following the equations described in Gray et al. (2018 and 2019). Combining  $\delta^{18}\text{O}$ , Mg/Ca  
115 and  $\Delta_{47}$  in foraminifera may therefore prove highly useful in palaeoceanographic studies.

116           The relationship between Mg/Ca and  $\Delta_{47}$  in modern planktonic foraminifera has been  
117 previously studied to investigate our ability to detect the potential biases associated to Fe-Mn  
118 oxide coatings, contamination and/or dissolution of foraminiferal tests (Breitenbach et al.,  
119 2018) in order to extract the best paleo-temperature estimates from non-biased  
120 measurements. However, the sensitivity of foraminiferal  $\Delta_{47}$  to salinity and pH has not been  
121 given much attention so far and still needs to be examined since a potential dependence of  
122  $\Delta_{47}$  on these chemo-physical parameters would potentially explain part of the differences  
123 observed between the  $\Delta_{47}$  and the Mg/Ca paleothermometers.

124           For the present paper, we measured Mg/Ca on the same set of samples and  
125 foraminiferal species used in the  $\Delta_{47}$  calibration of Peral et al. (2018). These data make it  
126 possible to explore the sensitivity of foraminiferal  $\Delta_{47}$  to salinity and pH and evaluate the  
127 potential interest and limits of combining  $\delta^{18}\text{O}$ , Mg/Ca- and clumped-temperatures to  
128 disentangle temperature, salinity- $\delta^{18}\text{O}_{\text{sw}}$ , and pH effects. In the process, we took advantage  
129 of re-calibrated clumped isotope data following cutting-edge methodological developments

130 to provide a revised version of the planktonic and benthic foraminiferal clumped isotope  
131 calibration of Peral et al. (2018), that could be used for future paleoceanographic studies.

132

## 133 **2. MATERIALS AND METHODS**

134

### 135 **2.1. Samples**

136

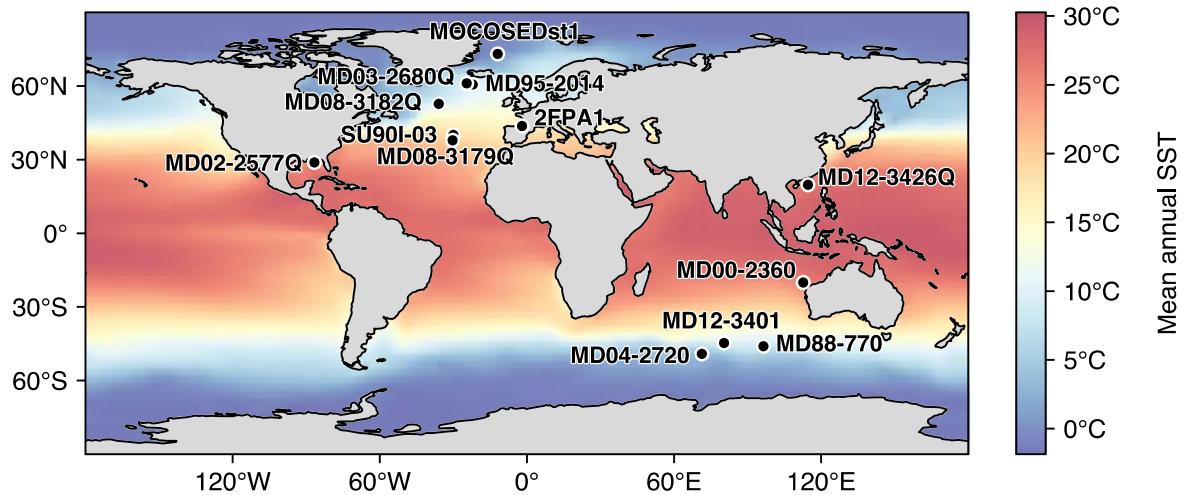
137 We used the same samples as those used in Peral et al. (2018), which are core-tops from  
138 twelve marine sedimentary cores from different oceanographic basins in the North Atlantic,  
139 Southern, Indian and Pacific Oceans (Fig. 1). All core-tops were chronologically constrained  
140 and are from the late Holocene (Peral et al., 2018). The location of samples, the water depths  
141 of the cores, the studied species and the ages are given in Table 1. We assume no changes in  
142 temperature, salinity, and pH over the late Holocene at our core sites and use modern  
143 hydrological atlases to estimate these data, at the location of our sites and at the living depths  
144 of the planktonic species studied here (see paragraph 2.4.). As discussed later, the recent  
145 warming and the addition of anthropogenic CO<sub>2</sub> to the surface ocean likely complicate the  
146 comparison of instrumental carbonate system measurements with core-top foraminiferal  
147 samples.

148 The core sites cover a wide range of seawater physico-chemical conditions, with  
149 temperatures ranging from 0.2 to 25 °C (for the planktonic only) and from -2 to 25 °C (including  
150 the benthic foraminifera), and with salinity ranging from 33.7 to 36.2 and pH from 7.7 to 8.1  
151 (both for planktonic only). The top 1 cm of each sediment core-top was collected and dried  
152 overnight at 50°C. The samples were wet sieved to collect the size fraction larger than 150 µm,  
153 and the residues were dried. To limit the potential size effects on Mg/Ca, we picked the  
154 planktonic foraminifera in narrow size ranges centered around the optimal size of each species  
155 (i.e., the size corresponding to the maximum abundance of adult shells). The optimal sizes are  
156 divided every ~50 µm (e.g., 200-250, 250-315, 315-355, 355-400, 400-450 and 450-500 µm).  
157 Each species have their size ranges (see details in Table 2).

158 Nine species of planktonic foraminifera and two species of benthic foraminifera were  
159 hand-picked under a binocular. For the Mg/Ca- $\Delta_{47}$  comparison, because of the differing  
160 carbonate chemistry controls on Mg/Ca in planktonic and benthic foraminifera (Lea, 1999;  
161 Elderfield et al 2006) we exclude the two benthic samples and only provide and discuss Mg/Ca

162 data from the planktonic foraminifera samples at the optimal size fractions. For the clumped-  
163 isotope calibration, we include the benthic foraminifera data, and a large range of size as was  
164 originally done in Peral et al. (2018).

165



166

167 **Figure 1:** Map showing the location of core-tops used in this study, with the mean annual SST  
168 from WOA13

169

## 170 2.2. Clumped isotopes

171

172 The clumped-isotope data were previously published in Peral et al. (2018). The  
173 methodology (from the cleaning protocol to the measurement) is described in Daëron et al.  
174 (2016) and Peral et al. (2018). A summary of the cleaning protocol steps is presented in the  
175 supplementary material (Fig. S1). In the present paper, we reprocessed our  $\Delta_{47}$  data in  
176 accordance with the new InterCarb - Carbon Dioxide Equilibrium Scale (I-CDES) and the  
177 associated data processing methods (Bernasconi et al., 2021; Daëron, 2021).

178

179 In previous studies, discrepancies between clumped isotope calibrations had been  
180 observed (e.g., Tripathi et al., 2010; Grauel et al., 2013). Thanks to an international effort,  
181 several laboratories conducted an intercalibration exercise in order to determine clumped  
182 isotope values of carbonate standards (ETH 1-4, IAEA-C1&2 and MERK; Bernasconi et al.,  
183 2021). This new standardization approach (I-CDES reference frame) results in internationally  
agreed calibrations (Anderson et al, 2021; Fiebig et al., 2021).

184 The  $\Delta_{47}$  values of our modern foraminifera (Peral et al., 2018) were normalized to the  
185 I-CDES reference frame (Bernasconi et al., 2021) using the carbonate standards ETH-1/2/3/4.  
186 Data processing was performed using the  $\Delta_{47}$ crunch library and the new pooled  
187 standardization approach, as described in Daëron (2021). The reprocessed  $\Delta_{47}$  calibration is  
188 now compared with the new and/or other recalculated calibrations and used for future  
189 paleoceanographic studies. The full dataset is provided in the supplementary material (Table  
190 S1).

191 The  $\Delta_{47}$  values were converted to temperatures using the Peral et al. re-calculated  
192 calibration. The temperature uncertainties were estimated by propagating (i) the external  
193  $\Delta_{47}$  reproducibility of our analytical sessions of measurements, based on repeated analyses of  
194 standards and samples and (ii) the uncertainties associated with respective calibrations.  
195 Recently, Anderson et al. (2021) have shown that when using the same standardization and  
196 data processing, re-evaluated  $\Delta_{47}$ -temperature calibrations obtained on various carbonate  
197 materials agree within the range of uncertainty. In terms of  $\Delta_{47}$ -temperature reconstructions,  
198 using Peral et al. (2018) re-calculated calibration (this paper), or using the unified calibration  
199 from Anderson et al. (2021), yield the same results. We found it important to provide in the  
200 present paper a revised calibration equation that is based on cutting-edge approaches of  $\Delta_{47}$   
201 standardization and processing methods (Bernasconi et al. 2021; Daëron, 2021) to serve for  
202 future studies based on the state-of-the-art standard values.

203

### 204 **2.3. Mg/Ca analyses and derived temperatures**

205

#### 206 **2.3.1. Mg/Ca measurements**

207

208 A total of 93 Mg/Ca analyses on 9 species of planktonic foraminifera were performed  
209 at the Laboratoire des Sciences du Climat et de l'Environnement (LSCE) using a PlasmaQuant  
210 ELITE Inductively coupled plasma mass spectrometry (ICP-MS) from Analytik Jena. One  
211 milligram of foraminiferal shells was hand-picked for each sample allowing to perform 3 to 4  
212 replicate analyses. We followed the cleaning protocol of Barker et al. (2003). Shells were  
213 crushed between two glass plates and the resulting fragments were put into acid-leached  
214 micro-vials. Fine material (i.e. clay) was removed through repeated ultrasonic cleaning with  
215 18.2 M $\Omega$  water and then ethanol. In order to remove potential organic contaminants, the



216 samples were then oxidized with alkali-buffered 1% H<sub>2</sub>O<sub>2</sub> solution for 10 minutes at 100°C.  
217 The final cleaning treatment consists in a rapid leaching with 0.001 M HNO<sub>3</sub>, before dissolution  
218 in 0.15 M HNO<sub>3</sub>. Samples are centrifuged immediately after dissolution and transferred to a  
219 new acid-leached centrifuge tube, leaving a residual ~ 10 µl, which helps exclude any  
220 remaining undissolved contaminants. Trace metal grade (NORMATOM) acids are used  
221 throughout.

222 A 10 µl aliquot of each sample was first analyzed in order to determine calcium  
223 concentrations. The samples were then diluted to a calcium concentration of 1mM Ca, to  
224 match that of the bracketing standards. Mg/Ca ratios were measured using a modified version  
225 of the method of Yu et al. (2005) against in-house standards prepared from single elementary  
226 solutions. Mg/Ca instrumental precision was determined based on multiple replicates of a  
227 standard solution of known Mg/Ca composition, with a long-term precision of 2% (2RSD).  
228 Analysis of external standard NIST RM 8301 (Foraminifera) using our method gives a value of  
229  $2.65 \pm 0.02$  (1SE), in excellent agreement with its published value of  $2.62 \pm 0.14$  (Stewart et  
230 al., 2020). The data are summarized in Table 2 and the full data set is provided in  
231 supplementary material (Table S2).

232

### 233 **2.3.2.** Correction of Mg/Ca for the effects of salinity and pH

234

235 We corrected our Mg/Ca values for pH and salinity effects based on the following  
236 procedure: 1) using species-dependent calibrations, we calculated at each core location the  
237 Mg/Ca values which are expected given the atlases-derived pH and salinity, and the δ<sup>18</sup>O-  
238 derived temperature, 2) at all the sites, we also calculated a pH- and salinity- normalized  
239 Mg/Ca values (Mg/Ca normalized) by setting pH=8 and salinity=35, and using the sample-  
240 specific oxygen isotopic-derived temperature; 3) the difference between the expected and  
241 normalized Mg/Ca values provide correction values at each site and for each species, (4) these  
242 correction values are then subtracted from our measured Mg/Ca values to cancel out the  
243 salinity and pH effects from our data, thus leaving only temperature as a control parameter.

244

245 Practically, for the first step of this procedure, we used the species-specific equations  
246 (Table 3) from Gray and Evans (2019) for *Globigerinoides ruber* and *Globigerina bulloides* to  
247 estimate the “expected” Mg/Ca values. For the species for which a specific calibration is not

248 available, we used the generic equation of Gray and Evans (2019). To the best of our  
249 knowledge, *N. pachyderma* is not pH sensitive (Tierney et al., 2019). Thus, no pH correction  
250 was applied to the Mg/Ca of this species, and it is corrected for salinity only.

251 The multi-parameter regression equations of Gray and Evans (2019) provide Mg/Ca as  
252 a function of the temperature, the salinity, and the pH of the sea water in which the  
253 foraminifera have grown:

$$254 \quad \text{Mg/Ca} = \exp ( a \times ( S - a ) + c \times T + d \times ( \text{pH} - e ) ) + f$$

255 Where a, b, c, d, e and f are constants, and T, S and pH are the temperature (in °C), the salinity  
256 and the pH of seawater during calcification. As said above, for each site and each species, we  
257 solved the regression equations using modern, atlas-derived pH and salinities, and the  
258 foraminifer  $\delta^{18}\text{O}$ -derived temperature (see details in section 2.4), and then proceed to steps  
259 2 to 4 (see above).

260

261

### 262 **2.3.3. Mg/Ca-derived temperatures**

263

#### 264 **2.3.3.1 Multi-species calibration equation from Anand et al. (2003)**

265

266 In order to compare Mg/Ca and clumped-isotope-derived temperatures, we first  
267 calculated the Mg/Ca-derived temperatures using the multi-species calibration of Anand et al.  
268 (2003) solved using our pH- and salinity- corrected Mg/Ca values. The estimated-Mg/Ca  
269 temperatures show a large difference when compared with the clumped-isotope-derived  
270 temperatures (see supplementary material, Fig. S2). We recalculated the multi-species Anand  
271 et al. (2003) calibration using the temperatures from the oxygen isotopic calibration of Kim  
272 and O'Neil (1997). This equation may provide a more robust basis for reconstructing  
273 temperature effects (Roche et al., 2018) than the modified, benthic-derived equation of  
274 Shackleton (1974) originally used in the Anand et al. (2003) study (see details in section 2.4.1).  
275 Following the same strategy as Anand et al. (2003), we only included the data from the 350 –  
276 500  $\mu\text{m}$  size-range and excluded the data from *Orbulina universa* and *Globigerinella*. We note  
277 that, as shown in Anand et al. (2003), the measured  $\delta^{18}\text{O}_{\text{calcite}}$  is up to  $\sim 1$  per mil too light in  
278 the wintertime compared to the value predicted using the measured sea surface temperature-  
279 and salinity-based  $\delta^{18}\text{O}_{\text{sw}}$  estimates at the Sargasso Sea sediment trap site. This is likely due to

280 a seasonal change in the  $\delta^{18}\text{O}_{\text{sw}}$ -salinity relationship at this site, which potentially introduces  
281 a substantial bias to the resulting Mg/Ca equation (Gray et al, 2018). The recalculated equation  
282 is presented in Table 3 and shown in supplementary material (Data Processing file).

283

#### 284 2.3.3.2 Mono species-specific equations

285

286 We first used calibration equations that were derived by linking Mg/Ca to temperature  
287 only. To the best of our knowledge, we chose the most adequate calibrations, considering the  
288 species, the size fraction, the oceanic region, and the cleaning protocol. For seven of the  
289 planktonic species studied in the present manuscript, we used the mono-specific equations of  
290 Anand et al. (2003). Unfortunately, the only available calibration for *Globorotalia menardii*  
291 was established using a cleaning protocol with a reductive step (Regenberg et al., 2010), which  
292 is known to lower the Mg/Ca ratio of foraminifera compared to the cleaning approach of  
293 Barker et al. (2003) that we used for the present paper (e.g., Pang et al., 2020). In the absence  
294 of a calibration for *Neogloboquadrina pachyderma* (dextral), we used the same calibration as  
295 the one developed for *N. pachyderma* (sinistral) (Vázquez Riveiros et al., 2016). The  
296 uncertainties were calculated by propagating the analytical errors, based on the long-term  
297 standard deviation of our standards and the uncertainties associated with the respective  
298 calibrations.

299 It is important to underline that, for internal consistency, the mono-species calibrations were  
300 corrected for local pH and salinity effects, as described in section 2.3.2. (i.e. species-specific  
301 equation of Gray and Evans (2019) with isotopic temperature, and salinity and pH from the  
302 atlases). For the Anand et al. (2003) calibrations, we used the *in situ* salinities available in  
303 Deuser and Ross (1989). The calibration of Regenberg et al. (2010) based on *G. menardii* was  
304 not corrected because we could not find the raw Mg/Ca data.

305

## 306 **2.4. Independent constraints on temperatures, salinity and pH from $\Delta_{47}$ and Mg/Ca ratios**

307

### 308 **2.4.1. Estimation of calcification temperatures**

309

310 In order to limit uncertainties associated to the imperfect knowledge of planktonic  
311 foraminifera ecology, numerous authors have used  $\delta^{18}\text{O}$ -derived temperatures instead of

312 atlas temperatures for the calibration of geochemical proxies (e.g. Anand et al., 2003;  
313 Mathien-Blard and Bassinot, 2009; Peral et al., 2018; Meinicke et al., 2020). Comparing  
314 WOA13 atlas temperatures and foraminifer  $\delta^{18}\text{O}$ -derived temperatures obtained using  
315 various calibration equations, Peral et al. (2018) suggested the use of the calibration equation  
316 of Kim and O'Neil (1997), modified for consistency by using an acid fractionation factor  
317 (difference of oxygen isotope ratio between the mineral (calcite) and the  $\text{CO}_2$  gas evolved from  
318 acidification with phosphoric acid) of 1.01025 (Eq. 1). The Kim and O'Neil (1997) calibration is  
319 then used to calculate the  $\delta^{18}\text{O}$ -derived temperatures in this study:

320

$$321 \quad 1000 \ln(\alpha_{\text{CC/W}}) = 18.03 \times 1000 / T - 32.17 \quad (\text{Eq. 1})$$

322

323 Where T is the isotopic temperature in Kelvin and  $\alpha_{\text{CC/W}}$  is the oxygen-18 fractionation factor  
324 between calcite and water, with:

325

$$326 \quad \alpha_{\text{CC/W}} = (1 + \delta^{18}\text{O}_{\text{C/SMOW}} / 1000) / (1 + \delta^{18}\text{O}_{\text{SW/SMOW}} / 1000) \quad (\text{Eq. 2})$$

327

328 Where  $\delta^{18}\text{O}_{\text{C/SMOW}}$  and  $\delta^{18}\text{O}_{\text{SW/SMOW}}$  correspond to foraminiferal calcite and seawater  $\delta^{18}\text{O}$   
329 relative to VSMOW. Following the recommendation of Marchitto et al. (2014),  $\delta^{18}\text{O}_{\text{C}}$  values  
330 for *Uvigerina* were adjusted by subtracting 0.47 ‰.

331 Seawater  $\delta^{18}\text{O}$  values at each core site were extracted from the gridded data set of  
332 LeGrande and Schmidt (2006). The same approach as the WOA-temperature extraction is  
333 followed (as described in Peral et al., 2018). Because one still does not know well the exact  
334 habitat depth and growth season of planktonic species and their spatial variability in relation  
335 to nutrient availability and physico-chemical conditions (i.e., Retailleau et al., 2011; Schiebel  
336 and Hemleben, 2017), we followed the same approach as Peral et al. (2018). We calculated  
337 the  $\delta^{18}\text{O}_{\text{SW}}$  of seawater in which foraminifera calcified by averaging at each site the gridded  
338  $\delta^{18}\text{O}_{\text{SW}}$  of LeGrande and Schmidt (2006) over species-specific living depth ranges. These depth  
339 ranges may vary across ocean basins. According to Tolderlund and Be' (1971) and Durazzi  
340 (1981), living depths in the North Atlantic Ocean range between 0 – 50 m for *G. ruber* and *O.*  
341 *universa*, and the depth range is 0-100m for *G. bulloides*, *G. truncatulinoides*, *G. menardii* and  
342 *G. inflata* (Steinke et al., 2005; Numberger et al., 2009, Rebotim et al 2017). For *N.*

343 *pachyderma*, the living depth is estimated from 0 to 200 m depth (Rebotim et al., 2017). In the  
344 Indian Ocean, Duplessy et al. (1981) placed the depth of calcification for all these species  
345 within and below the mixed layer, except for *G. ruber* and *G. menardii* which are believed to  
346 remain respectively at the surface and within the mixed layer (0–100 m). In the South China  
347 Sea, *G. ruber* and *G. menardii* are described as living near the surface and in the top 100 m,  
348 respectively (Pflaumann and Jian, 1999). Finally, the living depth of *O. universa* being very  
349 poorly constrained to the best of our knowledge, we assume that it lives everywhere at the  
350 same depth as in the North Atlantic Ocean (Rebotim et al., 2017). For benthic foraminifera (re-  
351 calibration of clumped isotope versus temperature), we must use the bottom  $\delta^{18}\text{O}_{\text{SW}}$  values.  
352 For the planktonic foraminifera, the mean  $\delta^{18}\text{O}_{\text{SW}}$  values averaged for the living depth of each  
353 species for each oceanic basin is considered. The uncertainty of  $\delta^{18}\text{O}_{\text{SW}}$  at each site was  
354 estimated as the quadratic sum of the site-specific standard deviation of  $\delta^{18}\text{O}_{\text{SW}}$  within the  
355 corresponding water depth and a constant error of 0.20 ‰ assigned to the GISS grid  
356 interpolation. Final uncertainties of the oxygen isotopic temperatures are propagated based  
357 on the  $\delta^{18}\text{O}_{\text{SW}}$  uncertainties and the external analytical error on  $\delta^{18}\text{O}$  values.

358 For *G. bulloides* and *O. universa*, we could also compare the reconstructed Mg/Ca-  
359 temperatures to  $\delta^{18}\text{O}$ -temperatures obtained using the species-specific  $\delta^{18}\text{O}$  calibrations from  
360 Bemis et al. (1998). This comparison is presented in Figure S3 and discussed in paragraph 4.2.

361

#### 362 **2.4.2.** Estimation of seawater salinity and pH

363

364 The seawater salinity values at each core-top location were extracted from the WOA13  
365 gridded data set (Zweng et al., 2013). As for the GISS  $\delta^{18}\text{O}_{\text{SW}}$  values (see above), for each ocean  
366 basin, we computed the seawater salinity in which the foraminifera calcified by averaging the  
367 atlas salinities over the living depth range known for each species. Uncertainties were  
368 estimated at each site as the quadratic sum of a nominal error of 0.20 arbitrarily assigned to  
369 the WOA13 data set and the site-specific standard deviation of salinity.

370 The seawater pH values at each core-top location and for each species living depth  
371 were extracted from the GLODAP 2020 data set (Olsen et al., 2020). Similarly, following the  
372 same strategy as for the GISS  $\delta^{18}\text{O}_{\text{SW}}$  and WOA13 salinity, we averaged the available GLODAP  
373 2020 data over the living depth-range published for each species. A pH uncertainty of 0.02

374 was assigned to GLODAP pH data (Olsen et al., 2020). We note that this only represents a  
375 'climatological' error. The use of climatological pH data is far from ideal because, due to the  
376 release of anthropogenic CO<sub>2</sub>, the surface ocean has acidified considerably since 1850. This  
377 has lowered the pH relative to the pre-industrial value, whereas the vast majority of  
378 foraminifera retrieved in the core top samples are likely to be of preindustrial age or older.  
379 This pH uncertainty represents a major source of uncertainty in our analysis and is a major  
380 hindrance to usefully constraining the sensitivity of foraminiferal proxies to the carbonate  
381 system using coretop material.

382

### 383 **3. RESULTS**

384

#### 385 **3.1. Clumped isotope dataset**

386

387 The clumped-isotope calibration using the same data set as Peral et al. (2018) is  
388 recalculated following the latest methodological developments (see section 2.2 for details).  
389 The recalculated clumped-isotope data range from 0.6976 ‰ to 0.5917 ‰ and cover a range  
390 of temperatures from -2.3 to 25.4 °C (oxygen isotopic temperatures from eq. 1 are used in the  
391 whole section; Table 2). As expected, the  $\Delta_{47}$  values increase with decreasing temperatures;  
392 the benthic foraminifera sample from the arctic (*C. wuellerstorfi* – MOCOSED-St1) shows the  
393 highest  $\Delta_{47}$  value, while planktonic foraminifer sample from one of the warmest sites *G. ruber*  
394 – MD00-2360) shows the lowest  $\Delta_{47}$  value.

395

#### 396 **3.2. Raw Mg/Ca dataset**

397

398 We only measured Mg/Ca for the planktonic foraminifera. Our raw Mg/Ca dataset  
399 ranges from 0.8 to 7.7 mmol/mol (Table 2 for the whole section) and covers a range of  
400 temperatures from -0.7 to 25.4 °C (temperatures for the whole section; Table 2). As expected,  
401 the cold-water dwelling foraminifera (*N. pachyderma* s. – MOCOSED st 1) show the lowest  
402 Mg/Ca values and the warm-water surface dwellers such as *G. ruber* and *O. universa* show the  
403 highest Mg/Ca values. Note the particularly high value (Mg/Ca =7.7 mmol/mol) obtained for  
404 *O. universa* . This species likely calcifies at a lower temperature than *G. ruber*, which  
405 nevertheless shows a raw Mg/Ca value of only 4.3 mmol/mol (sample of MD00-2360). Our

406 data therefore support previous observations that *O. universa* is characterized by unusually  
407 high Mg/Ca ratios (Lea, 1999; Anand et al., 2003).

408 The raw Mg/Ca ratios measured on the same samples and species, but for different  
409 size fractions, show a maximum difference of 0.4 mmol/mol between all the size fractions.

410

### 411 **3.3. Corrected Mg/Ca**

412

413 The raw Mg/Ca values are corrected for salinity and pH from atlas data, using the  
414 method as described in section 2.3.2. The corrected Mg/Ca, excluding *N. pachyderma*  
415 samples, ranges from 1.6 mmol/mol (Table 2) for *G. bulloides*-MD12-3401 that calcified at 5  
416 °C (isotopic temperatures, Table 2), to 4.9 for *G. ruber*-MD00-2360 that calcified at 24.8 °C  
417 (isotopic temperatures, Table 2). It is also noticeable that *G. bulloides* species still records high  
418 Mg/Ca values, as discussed in part 4.3. For a better comparison between our  $\Delta_{47}$  and Mg/Ca  
419 values, we test all subsequent analysis with and without *G. bulloides* in the dataset. The  
420 corrected Mg/Ca values for the species coming from the same core tops display a consistent  
421 relationship with calcification temperatures.

422

### 423 **3.4. Comparison of Mg/Ca-derived temperatures (multi-species and mono-species 424 equations) with $\delta^{18}\text{O}$ and $\Delta_{47}$ -derived temperatures**

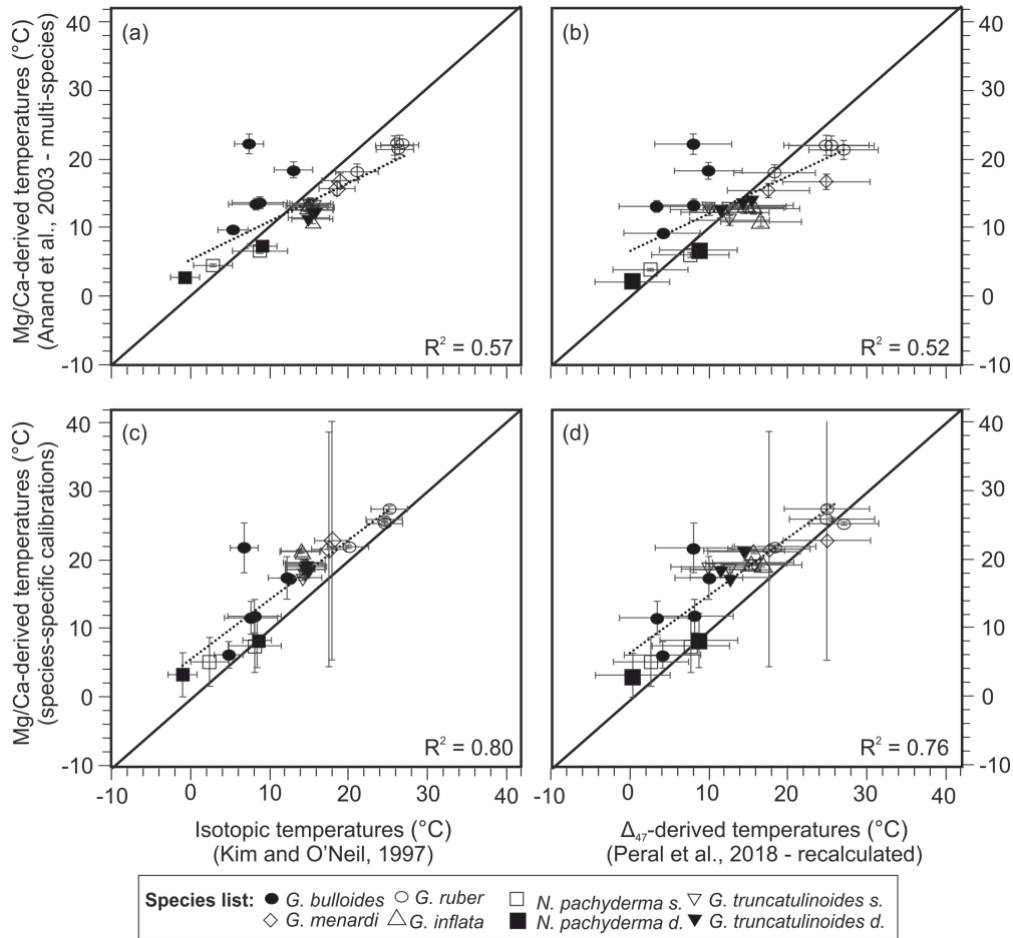
425

426 The Mg/Ca-derived temperatures were estimated using the recalculated multi-species  
427 calibration of Anand et al. (2003) and compared to the  $\delta^{18}\text{O}$ -temperatures (Fig. 2.a) estimated  
428 using Kim and O'Neil (1997) equation (eq. 1), as described in section 2.4.1. The Mg/Ca-  
429 temperatures for the species *G. bulloides* are systematically higher than the  $\delta^{18}\text{O}$ -derived  
430 temperatures, while most of the other species display lower Mg/Ca-derived temperatures  
431 (Fig. 2.a). A linear regression only explains 57 % of co-variance between the two thermometers  
432 (Fig. 2.a).

433 Then, the Mg/Ca-derived temperatures reconstructed using the multi-species  
434 calibration of Anand et al. (2003) are compared to the  $\Delta_{47}$ -derived temperatures obtained  
435 using the recalculated version of the foraminifer calibration equation of Peral et al. (2018; see  
436 section 2.3; Fig. 2.b). As was observed with the  $\delta^{18}\text{O}$ -temperatures, the *G. bulloides* species

437 show higher Mg/Ca-derived temperatures than those derived from  $\Delta_{47}$  and a linear regression  
 438 only explains 52 % of co-variance between the two thermometers (Fig. 2.b).

439 We then computed Mg/Ca-derived temperatures using mono-species calibrations.  
 440 These Mg/Ca-temperatures are in better agreement with  $\delta^{18}\text{O}$ -derived temperatures (Table  
 441 3; Fig. 2.c) and  $\Delta_{47}$ -derived temperatures (Fig. 2.d.), with regression equations explaining 80 %  
 442 and 76 % of co-variance. However, Mg/Ca-derived temperatures are always warmer than the  
 443 isotopic temperatures.



444  
 445 **Figure 2:** Comparison of temperature estimates obtained on 9 planktonic species. Top panels:  
 446 reconstructed Mg/Ca temperatures using the recalculated multi-species calibration of Anand  
 447 et al. (2003) compared to reconstructed  $\delta^{18}\text{O}$  temperatures, using Kim and O'Neil (1997) (a)  
 448 and  $\Delta_{47}$ -derived temperatures, using the recalculated calibration equation of Peral et al.  
 449 (2018) (this paper) (b). Bottom panel: reconstructed Mg/Ca derived temperatures using the  
 450 most adequate mono-specific calibrations compared to reconstructed  $\delta^{18}\text{O}$  temperatures,  
 451 using Kim and O'Neil (1997) (c) and  $\Delta_{47}$ -derived temperatures, using recalculated Peral et al.



452 (2018) calibration (d). Dotted black lines are linear regressions, the black solid lines are the 1:1  
 453 line. Uncertainties are at 2SE.

454

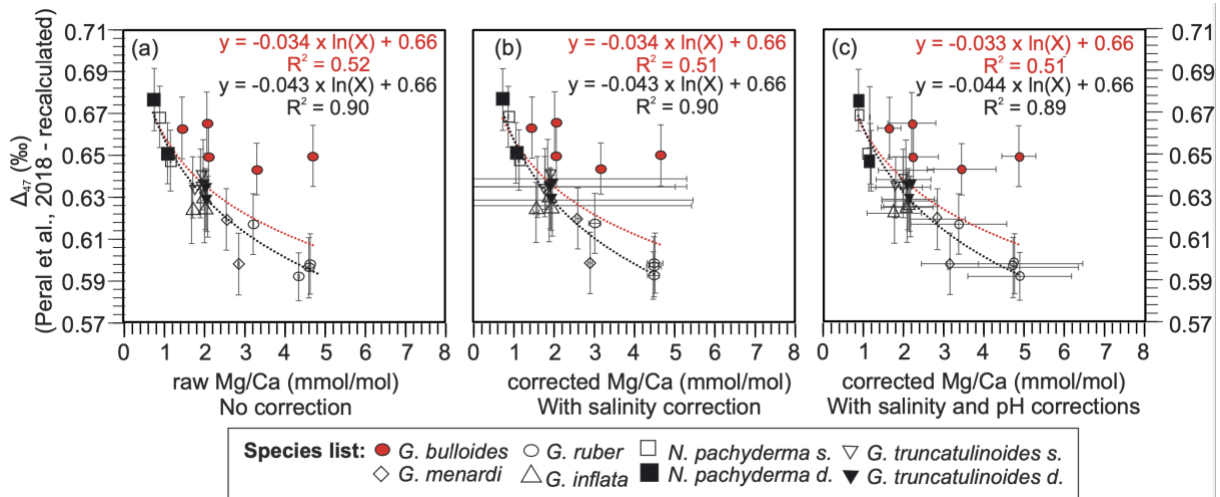
455 **3.5.  $\Delta_{47}$  values versus raw, corrected Mg/Ca values**

456

457 The  $\Delta_{47}$  values (recalculated from the raw data of Peral et al., 2018) are compared to  
 458 (1) the raw Mg/Ca values (Fig. 3.a – without *O. universa*), (2) the Mg/Ca values corrected for  
 459 seawater salinity only (i.e. setting d constant to zero in the correction equations from Gray  
 460 and Evans, 2019) (Fig. 3.b), and (3) the Mg/Ca values corrected for both seawater salinity and  
 461 pH salinity (Fig. 3.c).

462 The raw Mg/Ca data (without corrections) show a poor agreement with the  $\Delta_{47}$  values  
 463 (Fig. 3.a;  $R^2 = 0.52$ ). Similarly, poor agreement is observed using either "salinity" corrected  
 464 Mg/Ca or "salinity + pH" corrected Mg/Ca. " ( $R^2 = 0.51$  in Fig. 3.b & c). However, it should be  
 465 noted that without the *G. bulloides* samples, the agreements for the three comparisons  
 466 improve significantly with an  $R^2$  of 0.90, 0.90 and 0.89, respectively (Fig. 3.a&b&c).

467



468

469 **Figure 3:** Comparison of our recalculated foraminiferal  $\Delta_{47}$  values with raw Mg/Ca values  
 470 (uncorrected) (a), with corrected Mg/Ca for salinity only (b), and with corrected Mg/Ca for  
 471 salinity and pH (c). The Mg/Ca values are corrected using the equations from Gray and Evans  
 472 (2019), the salinity and pH from the atlas and the oxygen isotopic temperatures. The red  
 473 dotted logarithmic regressions are plotted for all the plots, including *G. bulloides* and the black  
 474 regressions are without *G. bulloides*. All the uncertainties are at 2SE.

475

476 **4. DISCUSSION**

477

478 **4.1. Updated foraminiferal clumped-isotope calibration**

479

480 The efforts of the clumped-isotope community have led to the establishment of an  
481 international standardization and a uniform measurement data processing, allowing  
482 robust/accurate comparisons between  $\Delta_{47}$  measurements performed in different laboratories  
483 (Bernasconi et al., 2021, and Fig. 4 therein). Following the newest methodological  
484 advancements in clumped isotope – new standard values and data processing (see details in  
485 section 3.2) - (Bernasconi et al., 2021; Daëron, 2021), we recomputed the multi-foraminiferal  
486 species calibration from Peral et al. (2018) (Fig. 4). The total least squares regression yields the  
487 following relationship:

488

$$489 \quad \Delta_{47} = A \times 10^3 / T^2 + B \quad \text{eq. 3}$$

490

491 Where  $A = 37.0$  and  $B = 0.181$

492 To compute the formal standard errors for this regression, we reformulate the  
493 equation 3 in terms of the barycenter of our  $(1/T^2_0)$  values, so that parameters A and  $B_0$  are  
494 statistically independent:

495

$$496 \quad \Delta_{47} = A*(T^{-2} - T_0^{-2}) + B_0 \quad \text{eq. 4}$$

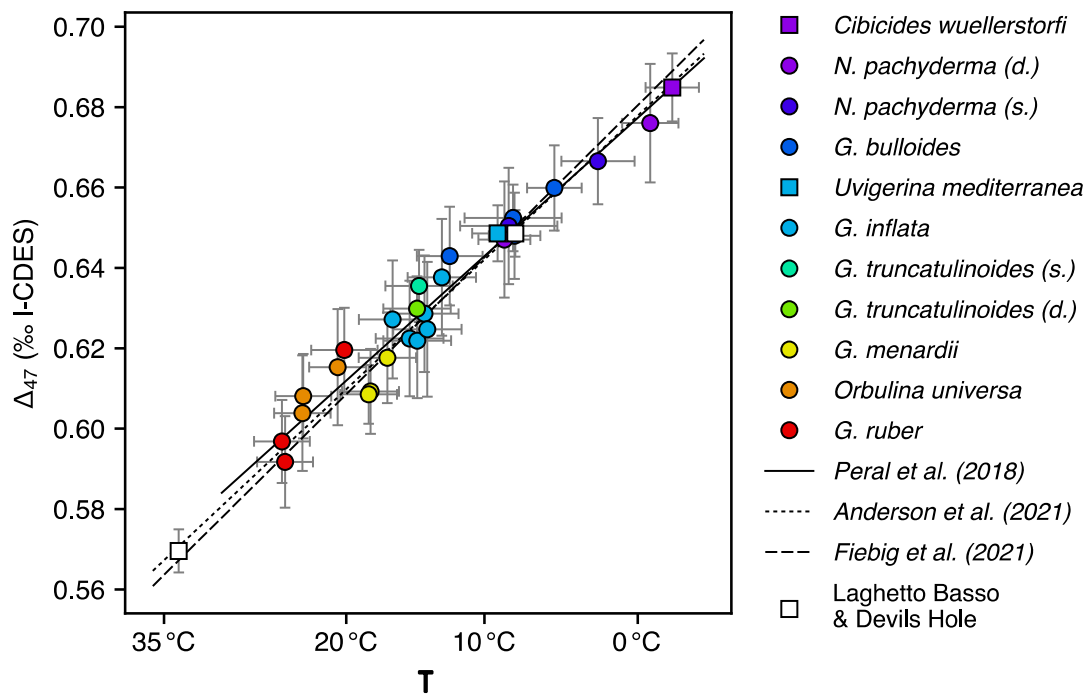
497

498 Where  $A = 37.0$  (SE = 2.0),  $B_0 = 0.636$  (SE = 0.0025) and  $T_0 = 285.1$  K

499

500 The conclusions drawn by Peral et al. 2018) based on the original data, are still valid –  
501 i.e. no apparent species-specific foraminiferal size and salinity effects (cf. Peral et al., 2018 for  
502 more details). The updated calibration established in the present paper is compared with the  
503 unified calibration of Anderson et al. (2021) and the precise inorganic calibration of Fiebig et  
504 al. (2021) (Fig. 4). A good agreement (in the range of 0.3 – 1.3 °C, within the calibration  
505 uncertainties) is observed between the three calibrations. This agreement between biogenic  
506 carbonates (this study) and inorganic carbonates (Anderson et al., 2021; Fiebig et al., 2021 and  
507 the slow-growing Laghetto Basso and Devils Hole calcite (Daëron et al., 2019; Anderson et al.,

508 2021)) confirms that using standardized protocols (Bernasconi et al., 2021; Daëron, 2021)  
 509 solves the large discrepancy between the calibrations (Anderson et al., 2021; Fiebig et al.,  
 510 2021). Also, this calibration constitutes the more precise equation based on foraminifera.  
 511 These observations allow a direct application of this calibration to foraminifera for  
 512 palaeoceanographic studies; this recalculated version of the calibration by Peral et al. (2018)  
 513 should be used instead of the original version for future paleoceanographic studies.



514  
 515 **Figure 4:** Recalculated  $\Delta_{47}$  values (mean and 2SE) compared to oxygen isotopic temperatures  
 516 (mean and 2SE) obtained with Kim and O’Neil (1997) for planktonic (circle) and benthic  
 517 (square) foraminifera samples, combining all size fractions (modified from Peral et al., 2018).  
 518 The new calibration regression corresponds to the black line (Peral et al., 2018 recalculated).  
 519 The recalculated foraminiferal calibration is compared to the slow-growing calcite from  
 520 Laghetto Basso and Devils Hole (from Anderson et al., 2021) and to calibrations of Anderson  
 521 et al. (2021) and Fiebig et al. (2021)

522  
 523 **4.2. Species specific effects on Mg/Ca-temperatures vs  $\Delta_{47}$ -temperatures comparison**  
 524

525 By comparing various paleothermometers we are able to better constrain the  
526 limitations of each of the methods and, within the framework of these limitations, try to  
527 extract as much meaningful climatic information as possible by combining those proxies.

528 The plot of Mg/Ca-temperatures vs  $\Delta_{47}$ -derived temperatures (Fig. 2.b) shows a larger  
529 scattering around the 1:1 line than the plot displaying Mg/Ca-temperatures vs  $\delta^{18}\text{O}$ -derived  
530 temperatures (Fig. 2.a). This larger scattering likely results from the higher uncertainties in the  
531 clumped-isotope-derived temperatures. The use of species-specific calibrations for Mg/Ca-  
532 derived temperatures improves the fit with the  $\Delta_{47}$ -derived temperatures, compared to the  
533 use of a multi-species calibration (Fig. 2.d vs Fig. 2.b). No species-specific calibration is  
534 necessary for clumped isotope as  $\Delta_{47}$  thermometer does not appear to be affected by species-  
535 specific effects (Tripathi et al., 2010; Grauel et al., 2013; Peral et al., 2018; Meinicke et al., 2020).

536 Although  $R^2$  values significantly increase when using species-specific Mg/Ca  
537 calibrations, the Mg/Ca-derived temperatures are systematically warmer than  $\delta^{18}\text{O}$ - and  $\Delta_{47}$ -  
538 derived temperatures (Fig. 2.b&d – linear regression lines). This is coherent with previous  
539 observations (Peral et al., 2020; Leutert et al., 2020).

540 No significant improvement is observed when species-specific calibrations are used to  
541 reconstruct temperatures from *G. bulloides* and *O. universa*  $\delta^{18}\text{O}$  (Bemis et al., 1998) (Figure  
542 S3). *G. bulloides* Mg/Ca data result in temperatures as high as 20 °C, showing up to 12 °C  
543 difference with the two isotopic thermometers (see discussion below in section 4.3.). One  
544 second explanation would be the dependance of Mg/Ca values on salinity and pH (Nürnberg  
545 et al., 1996; Kısakürek et al., 2008; Mathien-Blard and Bassinot, 2009, Gray et al., 2018; Gray  
546 and Evans, 2019). It has been shown that the  $\Delta_{47}$  in foraminifera is not affected by salinity  
547 (Tripathi et al., 2010; Peral et al., 2018), however, the pH dependence of the foraminiferal  $\Delta_{47}$   
548 thermometer has never been studied to this date. By comparing both foraminiferal- $\Delta_{47}$  and  
549 corrected-Mg/Ca temperatures, the potential effect of pH on clumped isotopes can be  
550 deciphered.

551

### 552 **4.3. *G. bulloides* species in Mg/Ca**

553

554 The relatively poor correlation between raw or corrected Mg/Ca and clumped isotope  
555 (Fig. 3a&b&c) chiefly results from particularly high *G. bulloides* Mg/Ca values and the high  
556 variability of *G. bulloides* data over a narrow  $\Delta_{47}$  range (Fig. 3a&b&c). The correlations

557 significantly improve when *G. bulloides* samples are excluded. The high Mg/Ca ratios  
558 measured in *G. bulloides* and their important variability are not explained by anomalous, local  
559 salinity or pH values. High *G. bulloides* Mg/Ca values could be likely explained by 1) diagenesis  
560 or metal coating, 2) pH effect on  $\delta^{18}\text{O}$  measurements or 3) the existence of different *G.*  
561 *bulloides* morphotypes and/or genotypes characterize by different temperature-driven Mg/Ca  
562 incorporation mechanisms.

563 1) Diagenesis or metal coating: The relationship between foraminiferal  $\Delta_{47}$  and raw Mg/Ca  
564 has been previously examined by Breitenbach et al. (2018). These authors suggested that the  
565 clumped isotope-Mg/Ca comparison could help identify potential problems and biases of the  
566 Mg/Ca-thermometer resulting from Fe-Mn oxide coatings, clay contamination and/or  
567 foraminiferal test dissolution. Our foraminifera samples are in a good state of preservation  
568 and do not suffer from dissolution (SEM pictures available in Peral et al., 2018). Additionally,  
569 the Fe/Ca and Mn/Ca values are low in our dataset, below the thresholds that lead to suspect  
570 a contamination problem (Boyle and Keigwin (1985); see supplementary material Table S2).  
571 Nevertheless, the *G. bulloides* sample showing the highest Mg/Ca value (sample from core  
572 MD95-2014) displays also an anomalously high Al/Ca content of 7337 mmol/mol compared to  
573 the other samples for which Al/Ca values are below 100 mmol/mol. For this sample,  
574 contamination by clay minerals is likely. Our observations suggest that the Fe-Mn oxide  
575 coatings, clay contamination (except for one sample) and/or foraminiferal test dissolution do  
576 not explain the too high Mg/Ca values of *G. bulloides* and the higher range of variability when  
577 compared with  $\Delta_{47}$  values.

578 2) pH effect on the  $\delta^{18}\text{O}$  measurements:  $\delta^{18}\text{O}$ -derived temperatures are used to correct  
579 the Mg/Ca; but the  $\delta^{18}\text{O}$  of *G. bulloides* may be affected by pH effect (Spero et al., 1997; Spero  
580 et al., 1999; Zeebe, 1999). As a result, the high corrected Mg/Ca may be due to not considering  
581 the pH effect on  $\delta^{18}\text{O}$ . However, if the Mg/Ca is corrected using the temperature from the  
582 WOA rather than by the  $\delta^{18}\text{O}$ -derived temperature, the conclusion is similar: high corrected  
583 Mg/Ca is obtained. The pH effect on *G. bulloides*  $\delta^{18}\text{O}$  cannot explain the high Mg/Ca ratio.

584 3) *G. bulloides* has been shown to present different morphotypes and also different  
585 genotypes (sometimes with a similar morphotype), these cryptic species can potentially live at  
586 different depths and have specific ecological niches (Osborne et al., 2020). The  $\Delta_{47}$  values of  
587 *G. bulloides* are in very good agreement with the other species used and do not show  
588 systematic biases (Fig. 3), suggesting that the singularity of *G. bulloides* data in the Mg/Ca. vs.

589  $\Delta_{47}$  only occur in Mg/Ca ratio. The  $\Delta_{47}$  SD of the *G. bulloides* measurements are good,  
590 suggesting that in any given sample, *G. bulloides* with the same morphotype and/or genotype  
591 were picked. However, we cannot exclude the possibility that different genotypes (with similar  
592 morphotype) were analyzed at different sites. More detailed studies on *G. bulloides* are  
593 essential to better understand the potential cryptic variability of this species and its impact on  
594 Mg/Ca incorporation.

595 In the rest of the article, *G. bulloides* samples are removed from the dataset to better  
596 compare the corrected Mg/Ca and the clumped isotope-derived temperatures.

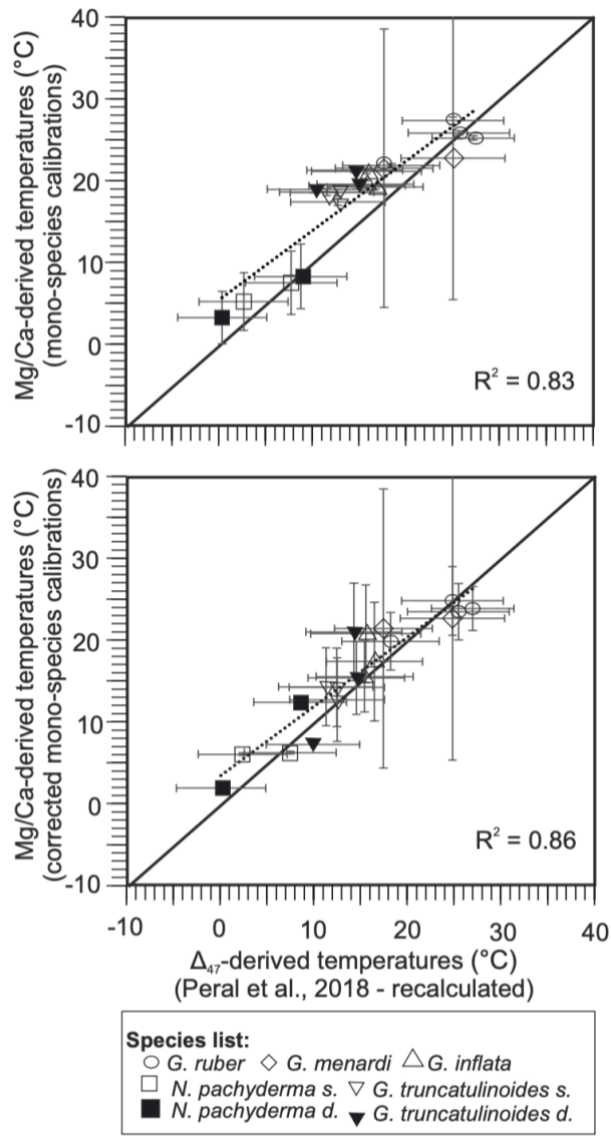
597

#### 598 **4.4. Salinity and pH effects on reconstructed Mg/Ca vs $\Delta_{47}$ temperatures**

599

600 Considering that the  $\Delta_{47}$  is independent of salinity and pH, and by correcting the Mg/Ca  
601 temperatures for each of these parameters, the observations made on figure 2 may be  
602 explained. In figure 5, we redraw the Mg/Ca-temperature vs.  $\Delta_{47}$ -temperature comparison of  
603 Figure 2d (i.e. obtained using the mono-specific calibration equations) but without *G.*  
604 *bulloides*. The mono-species Mg/Ca calibrations are corrected for salinity and pH (section  
605 2.3.3). Using this corrected-mono-species calibrations for Mg/Ca-derived temperature, the  
606 comparison with  $\Delta_{47}$ -derived temperatures is better; the regression line is close to the 1:1 line  
607 and explains 86% of the co-variance between both thermometers (Fig. 5). Thus, our results  
608 concur with observations from the geological record (Leutert et al, 2020; Meinecke et al 2021),  
609 that improved agreement between  $\Delta_{47}$ -derived and Mg/Ca-derived temperatures is observed  
610 when the influences of pH and salinity on Mg/Ca are accounted. This emphasizes the  
611 importance of correcting Mg/Ca values for non-thermal influences. However, it is noticeable  
612 that cold Mg/Ca-derived temperatures still show a slight difference with  $\Delta_{47}$ -derived  
613 temperatures. This could result from the small number of samples available and/or specific  
614 problems (e.g., effects of species,  $\text{CO}_3^{2-}$ ). More data is requested on the cold end member to  
615 better understand this potential difference.

616 The good agreement between the  $\Delta_{47}$ -derived temperatures and corrected Mg/Ca-  
617 derived temperatures provides further support that  $\Delta_{47}$  is not affected by salinity (Tripathi et  
618 al., 2010; Peral et al., 2018) and pH (or that the effect of pH is negligible).



619

620 **Figure 5:** Mg/Ca-derived temperatures using mono-species calibrations, compared to the  $\Delta_{47}$ -  
 621 derived temperatures using the recalculated Peral et al. (2018) calibration (a) and the Mg/Ca-  
 622 derived temperatures using the corrected Mg/Ca mono-species calibrations for salinity and  
 623 pH compared to the  $\Delta_{47}$ -derived temperatures using the recalculated Peral et al. (2018)  
 624 calibration (b). The dotted linear regression, excluding *O. universa* and *G. bulloides*, is plotted.  
 625 A line 1:1 is plotted in black; uncertainties are at 2 SE.

626

#### 627 4.5. The potential of combining Mg/Ca ratio, $\delta^{18}\text{O}$ and $\Delta_{47}$ for palaeoceanographic studies

628

629 The combination of  $\delta^{18}\text{O}$  and  $\Delta_{47}$  in foraminifera has been previously studied to  
 630 accurately reconstruct the signal of  $\delta^{18}\text{O}_{\text{sw}}$  even during glacial-interglacial scales (Rodriguez-  
 631 Sanz et al., 2021; Peral et al., 2020). Next, the comparison between Mg/Ca and  $\Delta_{47}$

632 systematically shows differences between the two thermometers in modern and fossil  
633 foraminifera. Breitenbach et al. (2018) showed that combining Mg/Ca and clumped isotopes  
634 data may help to detect possible dissolution and metal coating biases on the Mg/Ca-  
635 thermometer. When samples are not biased by contamination, dissolution or diagenesis, the  
636 combination of these two proxies has been used to estimate long-term variations in seawater  
637 Mg/Ca (Evans et al., 2018; Meinecke et al., 2021).

638 In the present study, we showed that salinity and pH lead to discrepancies between  
639 clumped isotope and Mg/Ca in planktonic foraminifera frequently used for paleoceanographic  
640 reconstructions (however, further work is needed for *O. universa* and *G. bulloides*). Because  
641 of the multi-parameter dependency of foraminiferal  $\delta^{18}\text{O}$ ,  $\Delta_{47}$  and Mg/Ca, the combination of  
642 these paleo-thermometers could provide us with more than just the estimates of past ocean  
643 temperatures. Theoretically, based on the Gray and Evans equation (2019), the pH could be  
644 reconstructed by (i) solving the Mg/Ca dependency to temperature using  $\Delta_{47}$ -derived  
645 temperatures and (ii) correcting for salinity using either the salinity estimated from sea level  
646 variations (Gray et al., 2019) or the salinity estimated from the combination of a thermometer  
647 ( $\Delta_{47}$ -temperature or  $\text{TEX}_{86}$  as in Leutert et al. (2020)) and  $\delta^{18}\text{O}$  (to obtain the  $\delta^{18}\text{O}_{\text{sw}}$ ).

648 We tested such an approach with our core-top dataset. Firstly,  $\delta^{18}\text{O}_{\text{sw}}$  was  
649 reconstructed by pairing  $\delta^{18}\text{O}$  and  $\Delta_{47}$  and using the equation 1 (Kim and O'Neil, 1997). Then  
650 salinity was reconstructed using modern salinity- $\delta^{18}\text{O}_{\text{sw}}$  relationships (section 2.4;  
651 supplementary material Fig. S4, at our site locations). Finally, we used our raw Mg/Ca, the  
652 estimated salinities and the clumped isotope temperatures to reconstruct pH values from the  
653 equations of Gray and Evans (2019). The reconstructed pH is compared to the pH extracted  
654 from the GLODAP 2020 data set (Olsen et al., 2020), by plotting their differences against the  
655 different species (Fig. 6). For each species, the differences between estimated- and atlas-pH  
656 ( $\Delta\text{pH}$ ) present a relatively good agreement, within the error bars, especially for *G. ruber* (Fig.  
657 6). Part of the differences can be explained by the inaccurate assumptions regarding the depth  
658 of life and the optimal developmental season of foraminifera species, thus leading to incorrect  
659 pH being extracted from the atlases. Additionally, another limitation of this approach is the  
660 salinity reconstruction that we applied. It requires to assume that, in the past, the regional  
661 relationships between  $\delta^{18}\text{O}_{\text{sw}}$  and salinity were the same as today. It is likely that in past  
662 climates, regional changes of evaporation/precipitation and isotopic fractionation during

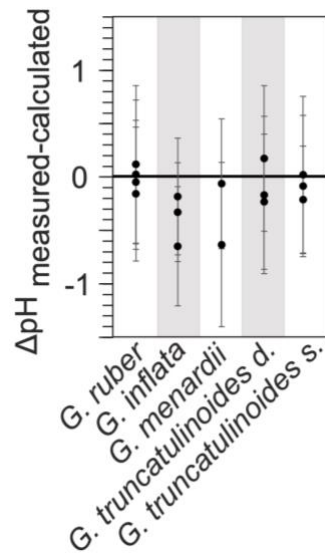


663 atmospheric transport of water vapor, lead to changes in the  $\delta^{18}\text{O}_{\text{sw}}$  – salinity relationship. On  
664 a global scale, these changes may have also altered the impact of ice sheet waxing/waning on  
665 the seawater  $\delta^{18}\text{O}_{\text{sw}}$ -salinity relationship. The extent and amount of sea ice may have also  
666 decoupled this  $\delta^{18}\text{O}_{\text{sw}}$ - salinity relationship (LeGrande and Schmidt, 2011). A direct application  
667 of the  $\delta^{18}\text{O}$  and  $\Delta_{47}$  combination is therefore not straightforward and other methods of salinity  
668 reconstruction should be used (Gray and Evans, 2019; Leutert et al., 2020).

669 Thus, despite the theoretical potential of the approach described above, it should be  
670 noted that the uncertainties in pH are large (at 2SE in Fig. 6), making the application of this  
671 approach challenging. It is important to note that these uncertainties are particularly large  
672 with respect to expected pH changes in the geological past (see discussion below). The  
673 uncertainties in the reconstructed pH range between 0.23 and 0.39, which is too high for  
674 useful paleoceanographic reconstruction and conversion to atmospheric  $\text{CO}_2$  concentration,  
675 since it has been estimated that pH variations over G-IG cycles are on the order of 0.15 (e.g.  
676 Hönisch and Hemming, 2005; Henehan et al., 2013), and by 0.2 units over the Miocene  
677 (Leutert et al., 2020)). In terms of propagation of errors, the estimated pH uncertainties are  
678 dominated by the uncertainties in the clumped isotope-derived temperatures. The  $\Delta_{47}$   
679 uncertainties need to be reduced by measuring more replicates or by improvements in mass  
680 spectrometry.

681 Further studies and technical improvements are needed to improve species-specific  
682 equations and better understand the dependence of Mg/Ca on salinity and pH, and to reduce  
683 the amount of material needed for  $\Delta_{47}$  measurements and decrease temperature  
684 uncertainties. It is also mandatory to improve our knowledge about past relationships  
685 between  $\delta^{18}\text{O}_{\text{sw}}$  and salinity. While we are not able yet to fully benefit from the combination  
686 of Mg/Ca,  $\delta^{18}\text{O}$  and  $\Delta_{47}$  ratios, the systematic use of these proxies is nonetheless useful to  
687 better understand these proxies, their biases and thus help their interpretations in  
688 paleoceanographic studies. Pairing these paleothermometers with the boron isotope pH  
689 proxy (e.g., Foster and Rae, 2016), which requires knowledge of temperature to calculate  $K_B$   
690 and pH, would allow for multiple independent constraints on past variations in pH and  
691 temperature.

692



693  
 694 **Figure 6:** the difference for all the species from our dataset (excluding *O. universa*, *G. bulloides*  
 695 and *N. pachyderma*) between the extracted pH from the atlas (GLOPAD 2020) and the  
 696 reconstructed pH, using the equations from Gray and Evans (2019) with the raw Mg/Ca, the  
 697  $\Delta_{47}$ -derived temperatures, and the combination of  $\delta^{18}\text{O}$  and  $\Delta_{47}$ -derived temperatures to  
 698 reconstruct the  $\delta^{18}\text{O}_{\text{sw}}$ . The uncertainties correspond to the uncertainties associated with the  
 699 reconstructed pH (2SE)

700

## 701 5. CONCLUSION

702

703 The Mg/Ca in 7 planktonic foraminifer species is affected by species, salinity and pH  
 704 effects (Gray et al., 2018). A strong correlation exists between  $\Delta_{47}$  and Mg/Ca data when the  
 705 later are corrected for salinity and pH effects with the  $\Delta_{47}$  values. The *G. bulloides*-Mg/Ca ratio  
 706 appear to show anomalously high values compared to the Mg/Ca- $\Delta_{47}$  relationship observed  
 707 for the other seven planktonic species. Another process(es) may affect Mg/Ca in this species  
 708 and additional investigation is needed to better understand what controls high Mg/Ca we  
 709 observe in this species.

710 The improved agreement observed between Mg/Ca- and  $\Delta_{47}$ -derived temperatures  
 711 when Mg/Ca values are corrected for salinity and pH suggests that the foraminiferal clumped  
 712 isotopes may only be temperature dependent. As such, the combination of the foraminiferal  
 713 Mg/Ca,  $\delta^{18}\text{O}$  and  $\Delta_{47}$ , could allow the temperature ( $\Delta_{47}$  thermometer), salinity (by combining  
 714  $\delta^{18}\text{O}$  and  $\Delta_{47}$ , to reconstruct the  $\delta^{18}\text{O}_{\text{sw}}$  and then, the salinity) and pH (the only remaining  
 715 unknown) of the past seawater to be determined. However, at present, the application of this

716 later approach is nontrivial. In particular, the  $\Delta_{47}$ -temperature uncertainties result in pH  
717 uncertainties higher than the expected pH changes in the geological record. Furthermore, the  
718 estimation of past salinity is also not straightforward. Finally, the species-specific Mg/Ca-pH  
719 sensitivity (Gray and Evans, 2019) adds an additional complication when applying the  
720 approach to extinct species.

721 This paper is also present an update of the foraminiferal clumped-isotope calibration  
722 of Peral et al. (2018), that benefits from the latest methodological developments (data  
723 processing and standardization) and can be directly applied to palaeoceanographic studies.

724

## 725 **References**

726

- 727 Anand P., Elderfield H. and Conte M. H. (2003) Calibration of Mg/Ca thermometry in  
728 planktonic foraminifera from a sediment trap time series. *Paleoceanography*, 18(2).
- 729 Anderson, N. T., Kelson, J. R., Kele, S., Daëron, M., Bonifacie, M., Horita, J., T. J. Mackey, C. M.  
730 John, T. Kluge, P. Petschnig, A. B. Jost, K. W. Huntinton, S. M. Bernasconi, Bergmann, K.  
731 D. (2021). A unified clumped isotope thermometer calibration (0.5–1100° C) using  
732 carbonate-based standardization. *Geophysical Research Letters*, e2020GL092069.
- 733 Barker S., Greaves M. and Elderfield H. (2003) A study of cleaning procedures used for  
734 foraminiferal Mg/Ca paleothermometry. *Geochemistry, Geophys. Geosystems* 4, 1–20.
- 735 Bemis, B. E., Spero, H. J., Bijma, J., & Lea, D. W. (1998). Reevaluation of the oxygen isotopic  
736 composition of planktonic foraminifera: Experimental results and revised  
737 paleotemperature equations. *Paleoceanography*, 13(2), 150-160.
- 738 Bernasconi, S. M., Daëron, M., Bergmann, K. D., Bonifacie, M., Meckler, A. N., Affek, H. P.,  
739 (n.d.). InterCarb: A community effort to improve inter-laboratory standardization of the  
740 carbonate clumped isotope thermometer using carbonate standards. *Geochemistry,*  
741 *Geophysics* and  
742 *Geosystems*. <https://doi.org/10.1002/essoar.10504430.410.1002/essoar.10504430.3e>  
743 [ms](https://doi.org/10.1002/essoar.10504430.3e)
- 744 Bernasconi S. M., Müller I. A., Bergmann K. D., Breitenbach S. F. M., Fernandez A., Hodell D.  
745 A., Jaggi M., Meckler A. N., Millan I. and Ziegler M. (2018) Reducing uncertainties in  
746 carbonate clumped isotope analysis through consistent 3 carbon- ate-based  
747 standardization. *Geochem. Geophys, Geosyst.*
- 748 Boyle, E. and Keigwin, L. (1985). Comparison of Atlantic and Pacific Paleochemical Records for  
749 the Last 215,000 Years - Changes in Deep Ocean Circulation and Chemical Inventories.  
750 *Earth and Planetary Science Letters*, 76:135–150.
- 751 Brand W. A., Assonov S. S. and Coplen T. B. (2010) Correction for the  $^{17}\text{O}$  interference in  
752  $\delta(^{13}\text{C})$  measurements when analyzing  $\text{CO}_2$  with stable isotope mass spectrometry  
753 (IUPAC Technical Report). *Pure Appl. Chem.* 82, 1719–1733. Available at:  
754 [https://www.degruyter.com/view/j/pac.2010.82.issue-8/pac-rep-09-01-05/pac-](https://www.degruyter.com/view/j/pac.2010.82.issue-8/pac-rep-09-01-05/pac-rep-09-01-05.xml)  
755 [rep-](https://www.degruyter.com/view/j/pac.2010.82.issue-8/pac-rep-09-01-05/pac-rep-09-01-05.xml)  
[09-01-05.xml](https://www.degruyter.com/view/j/pac.2010.82.issue-8/pac-rep-09-01-05/pac-rep-09-01-05.xml).
- 756 Breitenbach S. F. M., Mleneck-Vautravers M. J., Grauel A.-L., Lo L., Bernasconi S. M., Müller I.  
757 A., Rolfe J., Greaves M. and Hodell D. A. (2018) Coupled Mg/Ca and clumped isotope

758 analyses of foraminifera provide consistent water temperatures. *Geochim.*  
759 *Cosmochim. Acta* 236, 283–296.

760 Daëron, M., Blamart, D., Peral, M., & Affek, H. P. (2016). Absolute isotopic abundance ratios  
761 and the accuracy of  $\Delta 47$  measurements. *Chemical Geology*, 442, 83–96.

762 Daëron, M., Drysdale, R. N., Peral, M., Huyghe, D., Blamart, D., Coplen, T. B., ... & Zanchetta,  
763 G. (2019). Most Earth-surface calcites precipitate out of isotopic equilibrium. *Nature*  
764 *communications*, 10(1), 1–7.

765 Daëron, M. (2021). Full propagation of analytical uncertainties in  $\Delta 47$   
766 measurements. *Geochemistry, Geophysics, Geosystems*, 22(5), e2020GC009592.

767 de Villiers S., Greaves M. and Elderfield H. (2002) An intensity ratio calibration method for the  
768 accurate determination of Mg/Ca and Sr/Ca of marine carbonates by ICP-  
769 AES. *Geochemistry, Geophys. Geosystems* 3, n/a-n/a. Available at:  
770 <http://doi.wiley.com/10.1029/2001GC000169>.

771 Deuser, W. G., and E. H. Ross. 1989. Seasonally abundant planktonic foraminifera of the  
772 Saragossa Sea: Succession, deep-water fluxes, isotopic compositions, and  
773 paleoceanographic implications, *J. Foraminiferal Res.*, 19, 268–293

774 Eiler, J.M. (2007) “Clumped-isotope” geochemistry—the study of naturally-occurring, multiply-  
775 substituted isotopologues. *Earth Planet. Sci. Lett.* 262, 309–327.

776 Eiler, J.M. (2011) Paleoclimate reconstruction using carbonate clumped isotope thermometry.  
777 *Quat. Sci. Rev.* 30 (25–26), 3575–3588. [https://doi.org/10.1016/j.](https://doi.org/10.1016/j.quascirev.2011.09.001)  
778 [quascirev.2011.09.001](https://doi.org/10.1016/j.quascirev.2011.09.001)

779 Elderfield H., Gansen G. (2000). Past temperature and  $\delta^{18}\text{O}$  of surface ocean waters inferred  
780 from foraminiferal Mg/Ca ratios. *Nature*, 405, pp. 422–445

781 Elderfield, H., Vautravers, M., & Cooper, M. (2002). The relationship between shell size and  
782 Mg/Ca, Sr/Ca,  $\delta^{18}\text{O}$ , and  $\delta^{13}\text{C}$  of species of planktonic foraminifera. *Geochemistry,*  
783 *Geophysics, Geosystems*, 3(8), 1–13.

784 Elderfield H., Yu J., Anand P., Kiefer T. and Nyland B. (2006) Calibrations for benthic  
785 foraminiferal Mg/Ca paleothermometry and the carbonate ion hypothesis. *Earth Planet.*  
786 *Sci. Lett.* 250, 633–649.

787 Elderfield H., Greaves M., Barker S., Hall I. R., Tripathi A., Ferretti P., Crowhurst S., Booth L. and  
788 Daunt C. (2010) A record of bottom water temperature and seawater  $\delta^{18}\text{O}$  for the  
789 Southern Ocean over the past 440 kyr based on Mg / Ca of benthic foraminiferal  
790 *Uvigerina* spp. *Quat. Sci. Rev.* 29, 160–169. Available at:  
791 <http://dx.doi.org/10.1016/j.quascirev.2009.07.013>.

792 Evans, D., Brierley, C., Raymo, M. E., Erez, J., & Müller, W. (2016). Planktic foraminifera shell  
793 chemistry response to seawater chemistry: Pliocene–Pleistocene seawater Mg/Ca,  
794 temperature and sea level change. *Earth and Planetary Science Letters*, 438, 139–148.

795 Evans, D., Sagoo, N., Renema, W., Cotton, L. J., Müller, W., Todd, J. A., ... & Affek, H. P. (2018).  
796 Eocene greenhouse climate revealed by coupled clumped isotope-Mg/Ca  
797 thermometry. *Proceedings of the National Academy of Sciences*, 115(6), 1174–1179.

798 Erez, J. (2003). The source of ions for biomineralization in foraminifera and their implications  
799 for paleoceanographic proxies. *Reviews in mineralogy and geochemistry*, 54(1), 115–  
800 149.

801 Fiebig, J., Daëron, M., Bernecker, M., Guo, W., Schneider, G., Boch, R., Bernasconi, S., Jautzy,  
802 J., & Dietzel, M. (2021). Calibration of the dual clumped isotope thermometer for  
803 carbonates. *Geochimica et Cosmochimica Acta*, 312, 235–256.

804 Foster, G. L., & Rae, J. W. (2016). Reconstructing ocean pH with boron isotopes in  
805 foraminifera. *Annual Review of Earth and Planetary Sciences*, 44, 207-237.

806 Grauel A. L., Schmid T. W., Hu B., Bergami C., Capotondi L., Zhou L. and Bernasconi S. M. (2013)  
807 Calibration and application of the “clumped isotope” thermometer to foraminifera for  
808 high-resolution climate reconstructions. *Geochim. Cosmochim. Acta* 108, 125–140.  
809 Available at: <http://dx.doi.org/10.1016/j.gca.2012.12.049>.

810 Gray, W. R., Weldeab, S., Lea, D. W., Rosenthal, Y., Gruber, N., Donner, B., & Fischer, G. (2018).  
811 The effects of temperature, salinity, and the carbonate system on Mg/Ca in  
812 Globigerinoides ruber (white): A global sediment trap calibration. *Earth and Planetary  
813 Science Letters*, 482, 607–620. <https://doi.org/10.1016/j.epsl.2017.11.026>

814 Gray, W. R., & Evans, D. (2019). Nonthermal influences on Mg/Ca in planktonic foraminifera:  
815 A review of culture studies and application to the last glacial  
816 maximum. *Paleoceanography and Paleoclimatology*, 34(3), 306-315.

817 Hönisch, B., & Hemming, N. G. (2005). Surface ocean pH response to variations in pCO<sub>2</sub>  
818 through two full glacial cycles. *Earth and Planetary Science Letters*, 236(1-2), 305-314.

819 Henehan, M. J., Rae, J. W., Foster, G. L., Erez, J., Prentice, K. C., Kucera, M., ... & Elliott, T.  
820 (2013). Calibration of the boron isotope proxy in the planktonic foraminifera  
821 Globigerinoides ruber for use in palaeo-CO<sub>2</sub> reconstruction. *Earth and Planetary Science  
822 Letters*, 364, 111-122.

823 Kim S.-T. and O’Neil J. R. (1997) Equilibrium and nonequilibrium oxygen isotope effects in  
824 synthetic carbonates. *Geochim. Cosmochim. Acta* 61, 3461–3475. Available at:  
825 <http://linkinghub.elsevier.com/retrieve/pii/S0016703797001695>.

826 Kisakürek, B., A. Eisenhauer, F. Böhm, D. Garbe-Schönberg, and J. Erez (2008), Controls on  
827 shell Mg/Ca and Sr/Ca in cultured planktonic foraminiferan, Globigerinoides ruber  
828 (white), *Earth Planet. Sci. Lett.*, 273, 260–269, doi:10.1016/j.epsl.2008.06.026.

829 Kissel C., Laj C., Mulder T., Wandres C. and Cremer M. (2009) The magnetic fraction: A tracer  
830 of deep water circulation in the North Atlantic. *Earth Planet. Sci. Lett.* 288, 444–454.  
831 <https://doi.org/10.1016/j.epsl.2009.10.005>.

832 Kissel C., Van Toer A., Laj C., Cortijo E. and Michel E. (2013) Variations in the strength of the  
833 North Atlantic bottom water during Holocene. *Earth Planet. Sci. Lett.* 369, 248–259.

834 Lea, D., T. Mashiotta, and H. Spero (1999), Controls on magnesium and strontium uptake in  
835 planktonic foraminifera determined by live culturing, *Geochim. Cosmochim. Acta*, 63,  
836 2369–2379, doi:10.1016/S0016-7037(99)00197-0.

837 Lea DW (2014) Elemental and isotopic proxies of past ocean temperatures. *Treatise on  
838 Geochemistry*, eds Holland HD, Turekian KK (Elsevier, Amsterdam), 2nd Ed, pp 373–397.

839 Lear, C. H., Rosenthal, Y., & Slowey, N. (2002). Benthic foraminiferal Mg/Ca-  
840 paleothermometry: A revised core-top calibration. *Geochimica et Cosmochimica  
841 Acta*, 66(19), 3375-3387.

842 LeGrande A. N. and Schmidt G. A. (2006) Global gridded data set of the oxygen isotopic  
843 composition in seawater. *Geophys. Res. Lett.* 33, 1–5.

844 LeGrande, A. N., and Schmidt G. A. (2011), Water isotopologues as a quantitative paleosalinity  
845 proxy, *Paleoceanography*, 26, PA3225, doi:10.1029/2010PA002043

846 Leutert, T. J., Auderset, A., Martínez-García, A., Modestou, S., & Meckler, A. N. (2020). Coupled  
847 Southern Ocean cooling and Antarctic ice sheet expansion during the middle  
848 Miocene. *Nature Geoscience*, 13(9), 634-639.

849 Marchitto, T. M., Bryan, S. P., Curry, W. B., & McCorkle, D. C. (2007). Mg/Ca temperature  
850 calibration for the benthic foraminifer *Cibicidoides*  
851 *pachyderma*. *Paleoceanography*, 22(1).

852 Marchitto T. M., Curry W. B., Lynch-Stieglitz J., Bryan S. P., Cobb K. M. and Lund D. C. (2014)  
853 Improved oxygen isotope temperature calibrations for cosmopolitan benthic foraminifera.  
854 *Geochim. Cosmochim. Acta* 130, 1–11. [https://doi.org/ 10.1016/j.gca.2013.12.034](https://doi.org/10.1016/j.gca.2013.12.034).

855 Mathien-Blard E. and Bassinot F. (2009) Salinity bias on the foraminifera Mg/Ca thermometry:  
856 Correction procedure and implications for past ocean hydrographic reconstructions.  
857 *Geochemistry, Geophys. Geosystems* 10.

858 Meckler A. N., Ziegler M., Millán M. I., Breitenbach S. F. M. and Bernasconi S. M. (2014) Long-  
859 term performance of the Kiel carbonate device with a new correction scheme for  
860 clumped isotope measurements. *Rapid Commun. Mass Spectrom.* 28, 1705–1715.

861 Meinicke, N., Ho, S. L., Hannisdal, B., Nürnberg, D., Tripathi, A., Schiebel, R., & Meckler, A. N.  
862 (2020). A robust calibration of the clumped isotopes to temperature relationship for  
863 foraminifers. *Geochimica et Cosmochimica Acta*, 270, 160-183.

864 Meinicke, N., Reimi, M. A., Ravelo, A. C., & Meckler, A. N. Coupled Mg/Ca and clumped isotope  
865 measurements indicate lack of substantial mixed layer cooling in the Western Pacific  
866 Warm Pool during the last~ 5 million years. *Paleoceanography and Paleoclimatology*,  
867 e2020PA004115.

868 Mulitza, S., Boltovskoy, D., Donner, B., Meggers, H., Paul, A., Wefer, G. (2003) Temperature:  
869  $\delta^{18}\text{O}$  relationships of planktonic foraminifera collected from surface waters.  
870 *Palaeogeography, Palaeoclimatology, Palaeoecology*, 202(1–2), 143-152.  
871 [https://doi.org/10.1016/S0031-0182\(03\)00633-3](https://doi.org/10.1016/S0031-0182(03)00633-3).

872 Nummerger, L., Hemleben, C., Hoffmann, R., Mackensen, A., Schulz, H., Wunderlich, J. M., &  
873 Kucera, M. (2009). Habitats, abundance patterns and isotopic signals of morphotypes of  
874 the planktonic foraminifer *Globigerinoides ruber* (d'Orbigny) in the eastern  
875 Mediterranean Sea since the Marine Isotopic Stage 12. *Marine Micropaleontology*, 73(1-  
876 2), 90-104.

877 Nürnberg, D., J. Bijma, and C. Hemleben (1996), Assessing the reliability of magnesium in  
878 foraminiferal calcite as a proxy for water mass temperatures, *Geochim. Cosmochim.*  
879 *Acta*, 60, 803–814, doi:10.1016/0016-7037(95)00446-7.

880 Olsen, A., Lange, N., Key, R M., Tanhua, T., Bittig, H C., Kozyr, A., Álvarez, M., Azetsu-Scott, K.,  
881 Becker, S., Brown, P J., Carter, B R., da Cunha, L., Feely, R A., van Heuven, S., Hoppema,  
882 M., Ishii, M., Jeansson, E., Jutterström, S., Landa, C S., Lauvset, S K., Michaelis, P., Murata,  
883 A., Pérez, F F., Pfeil, B., Schirnick, C., Steinfeldt, R., Suzuki, T., Tilbrook, B., Velo, A.,  
884 Wanninkhof, R., Woosley, R. J. (2020). An updated version of the global interior ocean  
885 biogeochemical data product, GLODAPv2. 2020. *Earth System Science Data*, 12(4), 3653-  
886 3678.

887 Pang, X., Bassinot, F., & Sepulcre, S. (2020). Cleaning method impact on the Mg/Ca of three  
888 planktonic foraminifer species: A downcore study along a depth transect. *Chemical*  
889 *Geology*, 549, 119690.

890 Oomori, T., Kaneshima, H., Maezato, Y., Kitano, Y., 1987. Distribution coefficient of Mg<sup>2+</sup> ions  
891 between calcite and solution at 10–50°C. *Marine Chemistry* 20, pp. 327-336.

892 Osborne, E. B., Umling, N. E., Bizimis, M., Buckley, W., Sadekov, A., Tappa, E., ... & Thunell, R.  
893 C. (2020). A sediment trap evaluation of B/Ca as a carbonate system proxy in asymbiotic  
894 and nondinoflagellate hosting planktonic foraminifera. *Paleoceanography and*  
895 *Paleoclimatology*, 35(2), e2019PA003682.

896 Passey, B. H., & Henkes, G. A. (2012). Carbonate clumped isotope bond reordering and  
897 geospeedometry. *Earth and Planetary Science Letters*, 351, 223-236.

898 Peral M., Daëron M., Blamart D., Bassinot F., Dewilde F., Smialkowski N., Isguder G., Jorissen  
899 F., Kissel C., Michel E., Vázquez Riveiros, N. and Waelbroeck C. (2018) ScienceDirect  
900 Updated calibration of the clumped isotope thermometer in planktonic and benthic  
901 foraminifera. 239, 1–16.

902 Peral, M., Blamart, D., Bassinot, F., Daëron, M., Dewilde, F., Rebaubier, H., Nomade, S., Girone,  
903 A., Marimo, M., Maiorano, P., & Ciaranfi, N. (2020). Changes in temperature and oxygen  
904 isotopic composition of Mediterranean water during the Mid-Pleistocene transition in  
905 the Montalbano Jonico section (southern Italy) using the clumped-isotope  
906 thermometer. *Palaeogeography, Palaeoclimatology, Palaeoecology*, 544, 109603.

907 Petersen, S. V., Defliese, W.F., Saenger, C., Daëron, M., John, C. M., Huntington, K. W., Kelson,  
908 J. R., Bernasconi, S. M., Colman, A. S., Kluge, T., Olack, G. A., Schauer, A. J., Bajnai, D.,  
909 Bonifacie, M., Breitenbach, S. F. M., Fiebig, J., Fernandez, A. B., Henkes, G. A., Hodell, D.,  
910 Katz, A., Kele, S., Lohmann, K. C., Passey, B. H., Peral, M., Petrizzo, D. A., Rosenheim, B.  
911 E., Tripathi, A., Venturelli, R., Young, E. D., Wacker U., Winkelstern, I. Z. 2019. *Effects of*  
912 *Improved <sup>17</sup>O Correction on Inter-Laboratory Agreement in Clumped Isotope*  
913 *Calibrations, Estimates of Mineral-Specific Offsets, and Acid Fractionation Factor*  
914 *Temperature Dependence*. Special Issue of *Geochemistry, Geophysics, Geosystems*, 20,  
915 3495 – 3519

916 Piasecki, A., Bernasconi, S. M., Grauel, A., Hannisdal, B., Ho, S. L., Leutert, T. J., et al.  
917 (2019). Application of clumped isotope thermometry to benthic  
918 foraminifera. *Geochemistry, Geophysics, Geosystems*,  
919 2018GC007961. <https://doi.org/10.1029/2018GC007961>

920 Regenber, M., Steph, S., Nürnberg, D., Tiedemann, R., & Garbe-Schönberg, D. (2009).  
921 Calibrating Mg/Ca ratios of multiple planktonic foraminiferal species with  $\delta^{18}\text{O}$ -  
922 calcification temperatures: Paleothermometry for the upper water column. *Earth and*  
923 *Planetary Science Letters*, 278(3-4), 324-336.

924 Rebotim, A., Voelker, A. H., Jonkers, L., Waniek, J. J., Meggers, H., Schiebel, R., ... & Kucera, M.  
925 (2017). Factors controlling the depth habitat of planktonic foraminifera in the  
926 subtropical eastern North Atlantic. *Biogeosciences*, 14(4), 827-859.

927 Retailleau, S., Schiebel, R., & Howa, H. (2011). Population dynamics of living planktic  
928 foraminifers in the hemipelagic southeastern Bay of Biscay. *Marine*  
929 *Micropaleontology*, 80(3-4), 89-100.

930 Roche, D.M., C. Waelbroeck, B. Metcalfe, T. Caley, 2018. FAME (v1. 0): a simple module to  
931 simulate the effect of planktonic foraminifer species-specific habitat on their oxygen  
932 isotopic content. *Geoscientific Model Development* 11(9), 3587-3603.

933 Rodríguez-Sanz, L., Bernasconi, S.M., Marino, G. *et al.* Author Correction: Penultimate  
934 deglacial warming across the Mediterranean Sea revealed by clumped isotopes in  
935 foraminifera. *Sci Rep* 11, 17511 (2021). <https://doi.org/10.1038/s41598-021-96895-3>

936 Rosenthal, Y., Boyle, E. A., & Slowey, N. (1997). Temperature control on the incorporation of  
937 magnesium, strontium, fluorine, and cadmium into benthic foraminiferal shells from  
938 Little Bahama Bank: Prospects for thermocline paleoceanography. *Geochimica et*  
939 *Cosmochimica Acta*, 61(17), 3633-3643.

940 Schauble E. A., Ghosh P. and Eiler J. M. (2006) Preferential formation of  $^{13}\text{C}$ - $^{18}\text{O}$  bonds in  
941 carbonate minerals, estimated using first-principles lattice dynamics. *Geochim.*  
942 *Cosmochim. Acta* 70, 2510–2529.

- 943 Shackleton N. (1967) Oxygen isotope analyses and Pleistocene temperatures re-assessed.  
944 Nature 215, 15–17.
- 945 Shackleton N.J. (1974) Attainment of isotopic equilibrium between ocean water and  
946 benthonic foraminifera genus *Uvigerina*: isotopic changes in the ocean during the last  
947 glacial. Les méthodes quantitatives d'étude des variations du climat au cours du  
948 Pleistocène, Gif-sur-Yvette. Colloque international du CNRS, 219, pp. 203-210
- 949 Spero H.J., Bijma J., Lea D.W., Bermis B.E. (1997) Effect of seawater carbonate concentration  
950 on foraminiferal carbon and oxygen isotopes. *Nature*, 390, 497-500.
- 951 Spero H.J., Bijma J., Lea D.W., Russell, A.D. (1999) Deconvolving glacial ocean carbonate  
952 chemistry from the planktonic foraminifera carbon isotope record.  
953 F. Abrantes, A.C. Mix (Eds.), *Reconstructing Ocean History: A Window into the*  
954 *Future*, Kluwer Academic/Plenum Publishers, New York, 329-342
- 955 Steinke, S., Chiu, H. Y., Yu, P. S., Shen, C. C., Löwemark, L., Mii, H. S., & Chen, M. T. (2005).  
956 Mg/Ca ratios of two *Globigerinoides ruber* (white) morphotypes: Implications for  
957 reconstructing past tropical/subtropical surface water conditions. *Geochemistry,*  
958 *Geophysics, Geosystems*, 6(11).
- 959 Stewart, J. A., Christopher, S. J., Kucklick, J. R., Bordier, L., Chalk, T. B., Dapoigny, A., Douville,  
960 E., Foster, G. L., Gray, W. R., Greenop, R., Gutjahr, M., Hemsing, F., Henehan, M. J.,  
961 Holdship, P., Hsieh, Y., Kolevica, A., Lin, Y., Mawbey, E. M., Rae, J. W. B., Robinson, L. F.,  
962 Shuttleworth, R., You, C., Zhang, S., & Day, R. D. (2021). NIST RM 8301 boron isotopes in  
963 marine carbonate (simulated coral and foraminifera solutions): inter-laboratory  $\delta^{11}\text{B}$   
964 and trace element ratio value assignment. *Geostandards and Geoanalytical*  
965 *Research*, 45(1), 77-96.
- 966 Stolper D. A. and Eiler J. M. (2016) Constraints on the formation and diagenesis of  
967 phosphorites using carbonate clumped isotopes. *Geochim. Cosmochim. Acta* 181, 238–  
968 259.
- 969 Tierney, J. E., Malevich, S. B., Gray, W., Vetter, L., & Thirumalai, K. (2019). Bayesian calibration  
970 of the Mg/Ca paleothermometer in planktic foraminifera. *Paleoceanography and*  
971 *Paleoclimatology*, 34, 2005–2030. <https://doi.org/10.1029/2019PA003744>
- 972 Tripathi A. K., Eagle R. A., Thiagarajan N., Gagnon A. C., Bauch H., Halloran P. R. and Eiler J. M.  
973 (2010)  $^{13}\text{C}$ - $^{18}\text{O}$  isotope signatures and “clumped isotope” thermometry in foraminifera  
974 and coccoliths. *Geochim. Cosmochim. Acta* 74, 5697–5717. Available at:  
975 <http://dx.doi.org/10.1016/j.gca.2010.07.006>.
- 976 Tripathi, A. K., Hill, P. S., Eagle, R. A., Mosenfelder, J. L., Tang, J., Schauble, E. A., ... & Henry, D.  
977 (2015). Beyond temperature: Clumped isotope signatures in dissolved inorganic carbon  
978 species and the influence of solution chemistry on carbonate mineral  
979 composition. *Geochimica et Cosmochimica Acta*, 166, 344-371.
- 980 Urey, H.C., Lowenstam, H.A., Epstein, S. and McKinney, C.R. (1951): Measurements of  
981 paleotemperatures and temperatures of the Upper Cretaceous of England, Denmark  
982 and the southeastern United States. *Bull. Geo. Soc. of Am.*, 62: 399-416.
- 983 Vázquez Riveiros N., Govin A., Waelbroeck C., Mackensen A., Michel E., Moreira S., Bouinot T.,  
984 Caillon N., Orgun A. and Brandon M. (2016) Mg/Ca thermometry in planktic foraminifera:  
985 improving paleotemperature estimations for *G. bulloides* and *N. pachyderma* left.  
986 *Geochem. Geophys. Geosy.* 17, 1249– 1264. <https://doi.org/10.1002/2015GC006234>
- 987 Watkins, J. M., & Hunt, J. D. (2015). A process-based model for non-equilibrium clumped  
988 isotope effects in carbonates. *Earth and Planetary Science Letters*, 432, 152-165.



989 Whitaker J., Khrulev C., Huard D., Paulik C., Hoyer S., Mohr F. A., Marquardt C., Couwenberg  
990 B., Bohnet M., Brett M., Hetland R., Korenčiak M., Onu K., Helmus J. J., Hamman J.,  
991 Barna A., Koziol B., Kluyver T., May R., Smrekar J., Barker C., Davar G., Cournapeau  
992 D., da Silva D., Gohlke C., Kinoshita B. P. (2019). Unidata/netcdf4-python: version  
993 1.4.3.2 release (v1.4.3.2). Zenodo. <https://doi.org/10.5281/zenodo.2592291>  
994 Yu, J.M., Day, J., Greaves, M., Elderfield, H., 2005. Determination of multiple element/calcium  
995 ratios in foraminiferal calcite by quadrupole ICP-MS. *Geochem. Geophys. Geosyst.* 6,  
996 Q08P01. doi:10.1029/2005GC000964.  
997 Zeebe R.E. (1999). An explanation of the effect of seawater carbonate concentration on  
998 foraminiferal oxygen isotopes. *Geochim. Cosmochim. Acta*, 63, 2001-2007.  
999 Zweng, M.M, J.R. Reagan, J.I. Antonov, R.A. Locarnini, A.V. Mishonov, T.P. Boyer, H.E. Garcia,  
1000 O.K. Baranova, D.R. Johnson, D.Seidov, M.M. Biddle, 2013. *World Ocean Atlas 2013,*  
1001 *Volume 2: Salinity.* S. Levitus, Ed., A. Mishonov Technical Ed.; NOAA Atlas NESDIS 74, 39  
1002 pp.

1003 **Author contributions**

1004 MP and FB have designed the study. MP wrote the manuscript, and all co-authors help in the  
1005 writing. MD provided the python code to reprocess the clumped-isotope calibration. FB, DB,  
1006 MD and WG provided assistance in the interpretation of the clumped-isotope and/or Mg/Ca  
1007 data. JB, FJ, CK, EM and CW helped in the selection of the marine sediment cores and  
1008 foraminifer species. MP hand-picked the foraminiferal samples. MP and HR cleaned the  
1009 samples for the Mg/Ca measurements and HR and WG performed the Mg/Ca measurements.

1010

1011 **Acknowledgements**

1012 All authors thank the editor for his patience in the lengthy process of reviewing this article and  
1013 the 3 anonymous reviewers for their really useful comments that significantly improve the  
1014 manuscript. MP thanks the CEA for the financially support during her 3-years PhD fellowship  
1015 2015-2018.

**Table 1:** Core top locations and water depth with species considered in this study and chronological.

Cores	Latitude (°)	Longitude (°)	Water depth (m)	Species	Core-top cal. yrs BP (95% CL)	References
MOCOSDSt1	73.04	-11.93	1839	<i>Cibicides wuellerstorfi</i> ; <i>N. pachyderma s</i>	6317 (+150/-94) *	(1)
MD04-2720	-49.13	71.36	750	<i>N. pachyderma d</i>	n.a.	
MD12-3401	-44.69	80.4	3445	<i>G. bulloides</i>	< 4000 **	(2)
MD95-2014	60.59	-22.08	2397	<i>G. bulloides</i>	715 (+94/-149) *	(1)
MD08-3182Q	52.71	-35.94	1355	<i>N. pachyderma s</i> ; <i>G. bulloides</i>	500 (+40/-53) *	(3)
MD03-2680Q	61.06	-24.55	1812	<i>N. pachyderma d</i>	402	(4)
2FPA1	43.67	-2.00	664	<i>Uvigerina mediterranea</i>	< 4000 ***	(1)
SU90I-03	40.05	-30	2475	<i>G. bulloides</i>	2013 (+125/-120) *	(1)
MD08-3179Q	37.86	-30.3	2036	<i>G. ruber</i> ; <i>G. inflata</i> ; <i>G. truncatulinoides s</i> ; <i>G. truncatulinoides d</i>	4403 (+153/-121) *	(1)
MD12-3426Q	19.73	114.61	3630	<i>G. menardii</i> ; <i>O. universa</i>	1755 (+159/-139) *	(1)
MD00-2360	-20.08	112.67	980	<i>G. menardii</i> ; <i>O. universa</i> ; <i>G. ruber</i>	3622 (+135/-137) *	(1)
MD02-2577Q	28.84	-86.67	4076	<i>G. menardii</i> ; <i>O. universa</i> ; <i>G. ruber</i>	1107 (+110/-105) *	(1)

\* Age determined by radiocarbon dating

\*\* Age determined by stratigraphic control

\*\*\* Age determined by presence of Rose Bengal

(1) Peral et al., 2018; (2) Vazquez Riveiros et al., 2016; (3) Kissel et al., 2013 and (4) Kissel et al., 2009

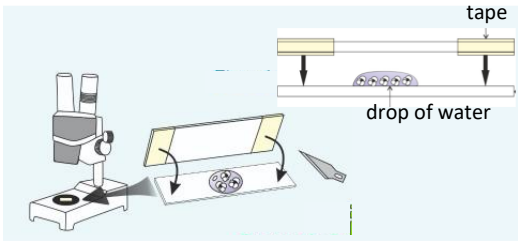
**Table 2:** Summary of the main results used in this study. The samples/species are represented with the optimal size fraction. The raw Mg/Ca values are presented, as well as the  $\delta^{18}\text{O}_c$  and the recalculated  $\Delta_{47}$  values with their associated uncertainties at 1SE. We also present the corrected Mg/Ca values for salinity and pH. Seawater salinity from WOA and pH from GLODAP 2020 (Olsen et al., 2020), are reported.

Core	Species	Optimal Size	$\delta^{18}\text{O}_c$ VPDB (‰)	SE	$\Delta_{47}$ (‰)	SE	Mg/Ca raw	SE	Mg/Ca corrected	SE	pH reconstructed	SE
MD08-3182	<i>G. bulloides</i>	250-315	1.77	0.1	0.6489	0.0074	2.10	0.006	2.24	0.309	7.941	0.27
MD08-3182	<i>G. bulloides</i>	315-355	1.87	0.1	0.665	0.0074	2.06	0.006	2.20	0.300	7.571	0.28
MD12-3401	<i>G. bulloides</i>	250-315	2.04	0.1	0.6626	0.0075	1.45	0.006	1.64	0.144	8.041	0.23
MD95-2014	<i>G. bulloides</i>	315-355	2.13	0.1	0.6492	0.0074	4.69	0.006	4.86	0.211	7.044	0.39
SU90-03	<i>G. bulloides</i>	250-315	1.59	0.1	0.6429	0.0063	3.30	0.006	3.44	0.427	7.570	0.30
MD08-3179	<i>G. inflata</i>	355-400	1.19	0.1	0.6286	0.0074	2.03	0.008	2.10	0.328	8.283	0.31
MD08-3179	<i>G. inflata</i>	400-450	1.08	0.1	0.6219	0.0073	1.68	0.008	1.76	0.339	8.747	0.29
MD08-3179	<i>G. inflata</i>	450-500	1.24	0.1	0.6247	0.0085	2.00	0.008	2.08	0.323	8.429	0.35
MD00-2360	<i>G. menardi menardi</i>	355-400	-0.37	0.1	0.5977	0.0075	2.85	0.004	3.15	0.354	8.741	0.37
MD00-2360	<i>G. menardi menardi</i>	400-450	-0.29	0.1	0.619	0.0074	2.55	0.004	2.84	0.346	8.170	0.34
MD00-2360	<i>G. ruber</i>	250-315	-1.76	0.1	0.5917	0.0058	4.34	0.008	4.88	0.643	8.262	0.32
MD02-2577	<i>G. ruber</i>	250-315	-1.33	0.1	0.5959	0.0073	4.59	0.008	4.71	0.813	8.099	0.37
MD02-2577	<i>G. ruber</i>	315-355	-1.46	0.1	0.5977	0.0073	4.63	0.008	4.75	0.847	8.029	0.37
MD08-3179	<i>G. ruber</i>	250-315	-0.08	0.1	0.6167	0.0073	3.21	0.008	3.37	0.597	7.988	0.33
MD08-3179	<i>G. truncatulinoides (d.)</i>	355-400	1.05	0.1	0.6424	0.0074	1.97	0.006	2.05	0.345	7.926	0.25
MD08-3179	<i>G. truncatulinoides (d.)</i>	400-450	1.14	0.1	0.6251	0.0074	2.09	0.006	2.16	0.336	8.331	0.34
MD08-3179	<i>G. truncatulinoides (d.)</i>	450-500	1.07	0.1	0.6278	0.0074	2.06	0.006	2.14	0.342	8.268	0.33
MD08-3179	<i>G. truncatulinoides (s.)</i>	355-400	1.08	0.1	0.638	0.0074	1.91	0.006	1.99	0.341	8.080	0.28
MD08-3179	<i>G. truncatulinoides (s.)</i>	400-450	1.07	0.1	0.6343	0.0074	1.90	0.006	1.98	0.342	8.184	0.30
MD08-3179	<i>G. truncatulinoides (s.)</i>	450-500	1.17	0.1	0.6342	0.0074	1.72	0.006	1.79	0.332	8.312	0.31
MD03-2680	<i>N. pachyderma (d.)</i>	200-250	1.73	0.1	0.647	0.0074	1.16	0.008	1.184	0.008		
MD04-2720	<i>N. pachyderma (d.)</i>	200-250	3.24	0.1	0.676	0.0075	0.76	0.008	0.87	0.008		
MD08-3182	<i>N. pachyderma (s.)</i>	200-250	1.76	0.1	0.6504	0.0074	1.09	0.006	1.17	0.006		
MOCOSSED	<i>N. pachyderma (s.)</i>	200-250	2.86	0.1	0.6678	0.0074	0.90	0.006	1.15	0.006		

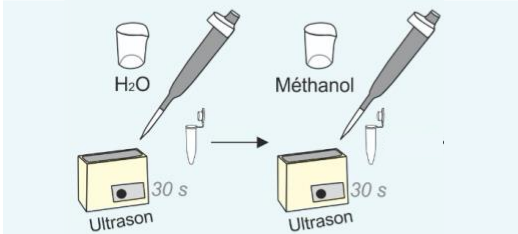
1 **Table 3:** Summary of all the Mg/Ca calibration used in this study: mono-specific species  
 2 calibrations, calibration with salinity and pH corrections and the salinity and pH corrected  
 3 multi-species calibration

Recalculated multi-species calibration from Anand et al., 2003					
Mg/Ca = B*exp(A*T)					
		Values	SE		
	A	0.0913	0.003		Recalculated in this study
	B	0.6109	0.002		
Mono-specific calibrations					
Mg/Ca = B*exp(A*T)					
		Values	SE	Size fraction	
<i>G. menardii</i>	A	0.091	0.012	355-400	Regenberg et al., 2009
	B	0.36	0.31		
<i>O. universa</i>	A	0.085	0.002	NA	Lea et al., 1999
	B	1.38	0.05		
	A	0.09		350-500	
	B	0.595	0.042		
<i>G. ruber</i>	A	0.09		250-350	Anand et al., 2003
	B	0.449	0.006		
	A	0.09		350-500	
	B	0.395	0.009		
<i>N. pachyderma s</i>	A	0.084	0.006	200-250	Vasquez Riveiros et al., 2016
	B	0.58	0.084		
<i>G. inflata</i>	A	0.09		350-500	
	B	0.299	0.005		
<i>G. truncatulinoides d.</i>	A	0.09		350-500	Anand et al., 2003
	B	0.359	0.008		
<i>G. truncatulinoides s.</i>	A	0.09		350-500	
	B	0.359	0.008		
<i>G. bulloides</i>	A	0.081	0.005	250-315	Elderfield and Ganssen. 2000 North Atlantic
	B	0.81	0.04		
	A	0.061	0.005	250-315	Elderfield and Ganssen. 2000 Southern Ocean
	B	0.996	0.038		
Mono-specific calibrations with SSS and pH corrections					
Mg/Ca=exp(A*(S - B) + C*T + D*(pH - E) + F					
		Values	SE		
<i>G. ruber</i>	A	0.036	0.006		
	B	35			
	C	0.061	0.005		
	D	-0.87	0.1		
	E	8	0		
	F	0.03	0.03		
<i>G. bulloides</i>	A	0.036	0.006		
	B	35			
	C	0.061	0.005		
	D	-0.88	0.12		
	E	8	0		
	F	0.21	0.04		Gray and Evans. 2019
<i>O. universa</i>	A	0.036	0.006		
	B	35			
	C	0.061	0.005		
	D	-0.51	0.11		
	E	8	0		
	F	0.77	0.48		
Multi-species	A	0.036	0.006		
	B	35			
	C	0.061	0.005		
	D	-0.73	0.07		
	E	8	0		
	F	0			

**Step 1**



**Step 2**



**Step 3**



**Cleaning protocol for clumped isotope in foraminifera**

**Step 1: Crush the foraminifera**

Gently crush foraminifera between two glass slides to open all chambers

**Step 2: remove clay**

Add milliQ water  
Remove the water  
Ultrasonic bath for 30s  
Repeat 3 times or more until water remains clear and colourless

Add methanol  
Ultrasonic bath for 30s  
Remove the methanol  
Repeat 2 time or more until the methanol remains clear and colourless

Remove the maximum of the methanol

**Step 3: Dry**

Dry at room temperature under a fume hood. Microtubes should be open but covered with aluminum foil to avoid dust contaminants

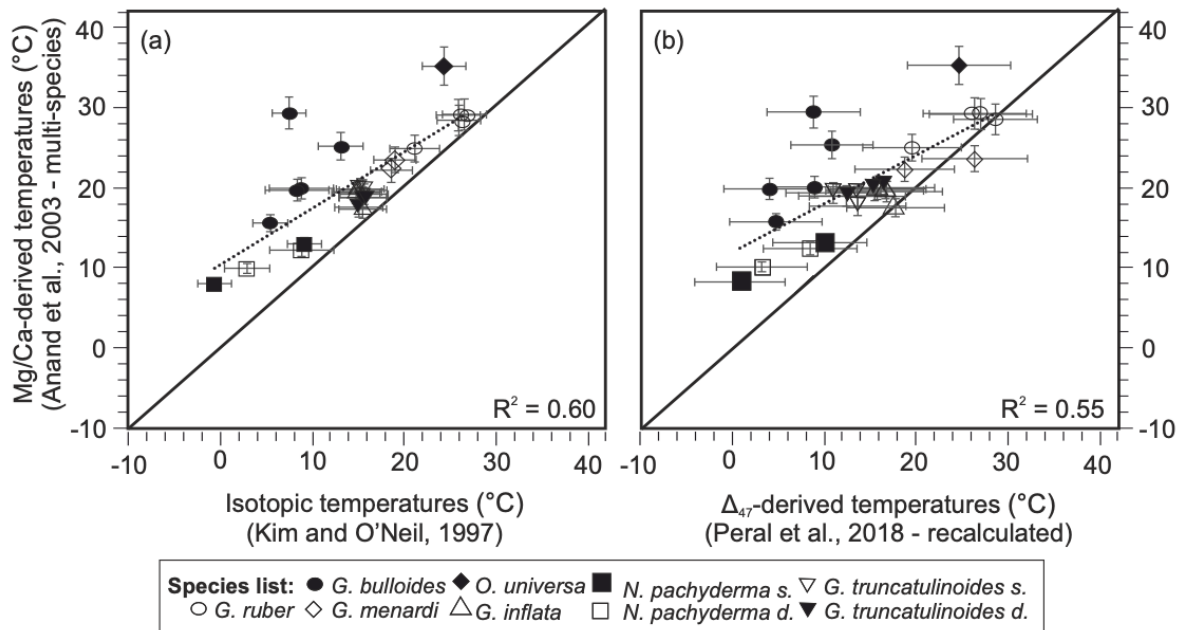
Equipment:

Microtubes, gloves, fume hood, microscope, 4 beaker (for water & dirty water and for methanol & dirty methanol), pipette and pipette tip (change for each sample or each step)

4  
5  
6

**Figure S1:** summary of the cleaning protocol steps for clumped isotope in foraminifera

7



8

9 **Figure S2:** reconstructed Mg/Ca temperatures using the original multi-species calibration of

10 Anand et al. (2003) compared to reconstructed  $\delta^{18}\text{O}$  temperatures, using Kim and O'Neil

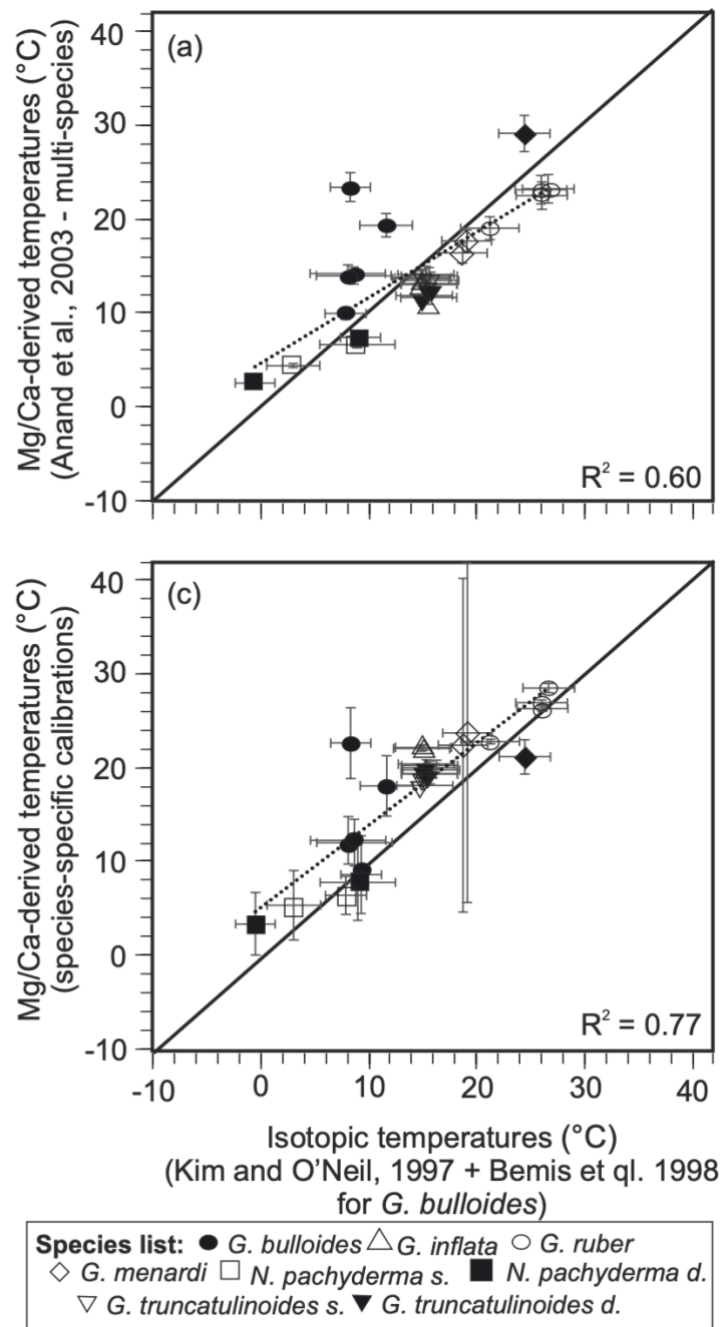
11 (1997) (a) and  $\Delta_{47}$ -derived temperatures, using recalculated Peral et al. (2018) (b) for 9 planktic

12 foraminifera. The linear regressions are the dotted black lines, a line 1:1 is in black, and the

13 uncertainties are at 2 SE. The Mg/Ca-derived temperatures are systematically higher than the

14 isotopic-derived temperatures.

15

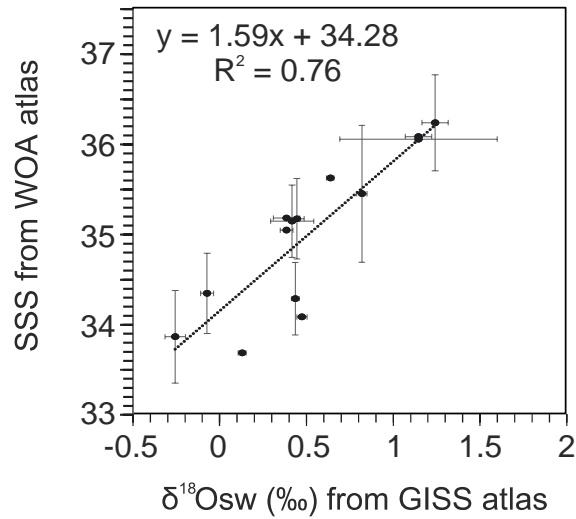


16

17 **Figure S3:** reconstructed Mg/Ca temperatures using the recalculated multi-species calibration  
 18 of Anand et al. (2003) compared to reconstructed  $\delta^{18}\text{O}$  temperatures, using Kim and O'Neil  
 19 (1997) (a) and reconstructed Mg/Ca derived temperatures using the most adequate mono-  
 20 specific calibrations compared to reconstructed  $\delta^{18}\text{O}$  temperatures, using Kim and O'Neil  
 21 (1997) and Bemis et al. (1998) calibration for *G. bulloides* (b). The linear regressions are the  
 22 dotted black lines, the 1:1 line is the black solid line, and the uncertainties are at 2 SE.

23





24  
 25 **Figure S4:** relationship between the seawater salinity from WOA 13 and the  $\delta^{18}\text{O}$  of the  
 26 seawater from GISS atlas for all our samples defined as core/species. For benthic foraminifera  
 27 we used the available bottom data and planktonic foraminifera we integrated data withing  
 28 the column water corresponding to the known living depths of each specie (see details in Peral  
 29 et al., 2018). The linear regressions are the dotted black lines, a line 1:1 is in black, and the  
 30 uncertainties are at 2 SE.

31

32 **Figure 1:** Map of core-top location used in this study, with the mean annual SST from WOA13

33

34 **Figure 2:** Comparison of temperature estimates obtained on 9 planktonic species. Top panels:

35 reconstructed Mg/Ca temperatures using the recalculated multi-species calibration of Anand

36 et al. (2003) compared to reconstructed  $\delta^{18}\text{O}$  temperatures, using Kim and O'Neil (1997) (a)

37 and  $\Delta_{47}$ -derived temperatures, using recalculated Peral et al. (2018) (b). Bottom panel:

38 reconstructed Mg/Ca derived temperatures using the most adequate mono-specific

39 calibrations compared to reconstructed  $\delta^{18}\text{O}$  temperatures, using Kim and O'Neil (1997) (c)

40 and  $\Delta_{47}$ -derived temperatures, using recalculated Peral et al. (2018) calibration (d). Dotted

41 black lines are linear regressions, the black solid lines are the 1:1 line. Uncertainties are at 2SE.

42

43 **Figure 3:** Comparison of our recalculated foraminiferal  $\Delta_{47}$  values with raw Mg/Ca values

44 (uncorrected) (a), with corrected Mg/Ca for salinity only (b), and with corrected Mg/Ca for

45 salinity and pH (c). The Mg/Ca values are corrected using the equations from Gray and Evans

46 (2019), the salinity and pH from the atlas and the oxygen isotopic temperatures. The red

47 dotted logarithmic regressions are plotted for all the plots, including *G. bulloides* and the black

48 regressions are without *G. bulloides*. All the uncertainties are at 2SE.

49

50 **Figure 4:** Recalculated  $\Delta_{47}$  values (mean and 2SE) compared to oxygen isotopic temperatures

51 (mean and 2SE) obtained with Kim and O'Neil (1997) for planktonic (circle) and benthic

52 (square) foraminifera samples, combining all size fractions (modified from Peral et al., 2018).

53 The new calibration regression corresponds to the black line (Peral et al., 2018 recalculated).

54 The recalculated foraminiferal calibration is compared to the slow-growing calcite from

55 Laghetto Basso and Devils Hole (from Anderson et al., 2021) and to calibrations of Anderson

56 et al. (2021) and Fiebig et al. (2021)

57

58 **Figure 5:** Mg/Ca-derived temperatures using mono-species calibrations, compared to the  $\Delta_{47}$ -

59 derived temperatures using the recalculated Peral et al. (2018) calibration (a) and the Mg/Ca-

60 derived temperatures using the corrected Mg/Ca mono-species calibrations for salinity and

61 pH compared to the  $\Delta_{47}$ -derived temperatures using the recalculated Peral et al. (2018)

62 calibration (b). The dotted linear regression, excluding *O. universa* and *G. bulloides*, is plotted.

63 A line 1:1 is plotted in black; uncertainties are at 2 SE.

64

65 **Figure 6:** the difference for all the species from our dataset (excluding *O. universa*, *G. bulloides*  
66 and *N. pachyderma*) between the extracted pH from the atlas (GLOPAD 2020) and the  
67 reconstructed pH, using the equations from Gray and Evans (2019) with the raw Mg/Ca, the  
68  $\Delta_{47}$ -derived temperatures, and the combination of  $\delta^{18}\text{O}$  and  $\Delta_{47}$ -derived temperatures to  
69 reconstruct the  $\delta^{18}\text{O}_{\text{sw}}$ . The uncertainties correspond to the uncertainties associated with the  
70 reconstructed pH (2SE)